SF 1

KfK 5377
August 1994

Long-Term Safety of Radioactive Waste Disposal:

Reaction of High Burnup Spent Fuel and UO_2 in Saline Brines at Room Temperature

B. Grambow, A. Loida, P. Dressler, H. Geckeis, P. Diaz, J. Gago, I. Casas, J. de Pablo, J. Giménes, M. E. Torrero

Institut für Nukleare Entsorgungstechnik
Institut für Heiße Chemie

Kernforschungszentrum Karlsruhe

KERNFORSCHUNGSZENTRUM KARLSRUHE

Institut für Nukleare Entsorgungstechnik
Institut für Heiße Chemie

KfK 5377

Long-Term Safety of Radioactive Waste Disposal:

Reaction of High Burnup Spent Fuel and UO_2 in Saline Brines at Room Temperature

B. Grambow, A. Loida, P. Dressler, H. Geckeis, P. Diaz*, J. Gago**, I. Casas***,
J. de Pablo***, J. Giménez***, M.E. Torrero***

*guest from CIEMAT, Madrid
**Empresa Nacional de Residuos Radioactivos S.A. (ENRESA)
***Universidad Politecnica de Cataluna (UPC)

Kernforschungszentrum Karlsruhe GmbH, Karlsruhe

Als Manuskript gedruckt
Für diesen Bericht behalten wir uns alle Rechte vor

Kernforschungszentrum Karlsruhe GmbH
Postfach 3640, 76021 Karlsruhe

ISSN 0303-4003

These works were performed in part under contract No.

F12W - 0055

with the Commission of the European Communities (Brussels)

ABSTRACT

In order to determine the long-term performance of spent fuel during direct disposal. high burnup fuel (50 MWd/kg U) has been exposed for 500 days to non-buffered saline solutions and to deionized water under static, anaerobic conditions at 25 °C. In the absence of saturation effects (large solution volumes) a dissolution rate of 0,3 % p.a. has been measured. Under more realistic conditions of large sample surface areas and small solution volumes, reaction rates were found to be orders of magnitude lower. The pH values remained neutral to slightly alkaline. Radiolysis did not lead to an oxidation of the solution. The releases of Sr90, Tc99, Np237 and Sb125 were controlled by the rate of dissolution of the fuel matrix, whereas the solution concentrations of U, Pu, Am and REE were governed by sorption and solubility effects. In the presence of iron, radiolytically produced oxygen has been consumed by iron corrosion and sorption on iron corrosion products effectively reduced the solution concentrations of most radionuclides. Studies of the corrosion of unirradiated UO_2 have shown strong indications for the formation of U(IV) hydroxide. Under oxidizing conditions, only in few cases solubility limits were reached. In the determination of UO_2 corrosion rates one has to distinguish between the initial fast process of dissolving an oxidized surface layer of $UO_{2,6}$ and the process of dissolution of the uranium dioxide beneath and the formation of a new layer of $UO_{2,4}$. Under anaerobic conditions reaction rates were significantly lower than under oxidizing conditions.

KURZFASSUNG

Reaktion von hochabgebranntem Kernbrennstoff und von UO_2 in salinen Lösungen bei Raumtemperatur

Zur Bewertung der Langzeitstabilität im Hinblick auf die Direkte Endlagerung wurde **hochabgebrannter Kernbrennstoff** (50 MWd/kg U) unter statischen anaeroben Bedingungen in Kontakt gebracht mit ungepufferten Salzlösungen und mit reinem Wasser für Zeiträume über 500 Tage bei 25°C. Unter Ausschluß von Sättigungseffekten (große Lösungsvolumina) wurde eine Auflösungsrate von 0,3% pro Jahr gemessen. Unter realistischen Bedingungen großer Brennstoffoberflächen und kleiner Lösungsvolumina wurden um Größenordnungen kleinere Reaktionsraten gemessen. Die pH-Werte in den Lösungen blieben bei fortschreitender Reaktion neutral bis leicht alkalisch. Radiolyse führte nicht zu einer Oxidation der Lösung. Die Freisetzung von Sr90, Tc99, Np237 und Sb125 wird durch die Rate der Auflösung der UO_2-Matrix limitiert, während die Lösungskonzentrationen von U, Pu, Am und SEE durch Sorptions- und Löslichkeitseffekte bestimmt werden. In Gegenwart von Eisen wird der gesamte, durch Radiolyse entstehende freie Sauerstoff bei der Korrosion des Eisens verbraucht und durch Sorption an Fe-Korrosionsprodukten reduzierten sich die Lösungskonzentrationen der untersuchten Nuklide erheblich. Korrosionsversuche mit **unbestrahltem UO_2** zeigen, daß sich unter reduzierenden Bedingungen die Bildung von U(IV)-Hydroxiden andeutet, während unter oxidierenden Bedingungen nur in wenigen Fällen Löslichkeitsgrenzen erreicht wurden. Bei der Ermittlung von Auflösungsraten muß zwischen der schnellen Auflösung einer oxidierten Oberflächenschicht der Proben von einer Zusammensetzung $UO_{2.66}$, und der langsamen Auflösung des unter der $UO_{2.6}$ liegenden Urandioxids unter Bildung einer stationären Oberflächenschicht mit der Zusammensetzung $UO_{2.4}$ unterschieden werden. Unter anaeroben Bedingungen lagen die Reaktionsraten deutlich unter denen bei oxidierenden Bedingungen.

Contents

LONG - TERM SAFETY OF RADIOACTIVE WASTE DISPOSAL

According to the federal waste management concept, similarly as in most other countries producing nuclear energy, solid high-level radioactive wastes such as HLW-glass and /or spent fuel shall be disposed in deep geological formations. Emphasis in evaluating the suitability of a disposal site is on the saltdome in Gorleben. The release of hazardous quantities of radionuclides into the biospere shall be excluded. For this purpose several independent barriers ("multibarrier concept") shall limit the transport of ground water to and from the waste and shall also reduce the mobility of radionuclides by retention within stable waste matrices, by remineralization and sorption processes. The innermost barrier is an engineered system consisting of the waste form "high-level waste glass" or "spent nuclear fuel", the packaging material (e.g., steel container) and the backfilling material (e.g., salt chippings, clay, apatite). In addition, geoengineered barriers (e.g.,filling material, dams) and the geological barrier (host rock, overburden) contribute to safety by delaying the transport of the radionuclides (e.g., by sorption). Without comprehensive knowledge of the performance of each of the various barriers under disposal conditions long-term safety of the repository cannot be guaranteed. Special attention is directed on the dissolution or corrosion behavior of the high active waste forms governing the source term of radionuclide remobilization. This mobilization of radionuclides is a prerequisite of further radionulide migration in the repository. Released radionuclides may subsequently become reimmobilized within newly formed mineral phases (secondary reaction products) or by sorption on surfaces of host rock or engineered materials. For assessing of the performance of the engineered barrier system, dissolution, remineralisation and migration phenomena must be analysed simultaneously.

Performance of the engineered barrier system

Experimental programmes which are conceived for a long term and aimed at performance assessment of glass and spent fuel are currently being conducted at KfK(INE). In order to understand the behavior of individual radionuclides, the corrosion behavior of the waste forms is studied in the context of basic studies on the chemistry (solubility, complexation,...) of important radionuclides (in particular the actinides) in diluted solutions and concentrated brine solutions. Results obtained in this research project will be published in a number of KfK-reports related to the subject of "long-term safety of radioactive waste disposal".

The ongoing work is mainly focused on analysing the corrosion behavior of real highly radioactive waste products under conditions which constitute the worst case in a repository in salt formations. However, for reasons of comparison, also the behavior in other formations (e.g. granite) is investigated. The used waste products are

- high-level waste borosilicate glass R7T7, the composition of which corresponds to the glass, produced by the COGEMA for the German base load customers,
- high burnup UO_2 fuel (burnup > 50 MWd/kg U) from the Biblis and Gösgen (Switzerland) nuclear power plants.

The behaviour of the waste forms in contact with solutions is evaluated on the basis of the type and amount of radionuclides released, the gaseous reaction products and the structural change of the solid phases (e.g., decomposition of the microstructures, formation of secondary phases). Corrosion mechanisms, rate laws and processes governing release of individual radionuclide (sorption, solubility, etc.) are to be determined.

The interaction of simoultaneous corrosion of container material and of the waste forms is investigated inserting container materials in the glass and spent fuel corrosion experiments. Additionally, separate container corrosion studies are performed for the determination of rate laws, container life times and for the improvement of container concepts.

Our work serves the long term purpose of developing models by means of which the contribution of the engineered barrier system to repository long.term safety can be assessed. The significance of individual experimental observations can only be evaluated in the general context. The relevance of laboratory findings for the natural system must be assessed as well as the validity of the models developed. Whether or not the total dissolution of the waste forms after many thousand of years would be detrimental to overall safety of the disposal system, or whether long and slow transport paths provide sufficient protection, can only be answered, based on an overall safety analyis, considering all significant individual processes and barrier functions adequately.

GENERAL OBJECTIVES AND SCOPE OF THE PROJECT

The research project aims at characterization and qualification of the chemical durability of unprocessed high burnup UO_2 fuel as a barrier against radionuclide release for disposal in salt formations. The reaction behavior of the fuel with saline brines is going to be studied as a function of time, temperature, redox potential and surface area in order to give insight into the corrosion mechanism and sources of release. Additionally, the solubility of unirradiated UO_2 in salt brines is studied for comparison with the reaction behavior of the irradiated material, in order to identify radiolysis and burnup effects in the degradation of the fuel matrix. Eventually the ongoing work will provide a basis for modelling, bridging over the gap between experimental results and performance assessment for long-term storage of the fuel in a repository in salt formations in the case of brine intrusion.

SUMMARY

As part of a research project on the long-term safety of radioactive waste disposal (see below), with respect to direct disposal the stability of spent fuel is studied as a barrier against radionuclide release. In the frame of a joint german (KfK)-spanish (ENRESA) project of the European Union, **high-burnup spent fuel** (>50 MWd/kgU) was exposed to non-buffered NaCl solutions and deionized water under static anaerobic conditions. These corrosion experiments shall contribute to the understanding and quantification of processes, which may control radionuclide release under conditions of eventual water access to the fuel in a repository. The accumulated corrosion time was about 500 days for experiments performed at room temperature. Experiments at 150°C were started. Gas phase and leach solutions were analyzed. By using various dimensions of spent fuel sample with surface areas differing by more than four orders of magnitude a range of reaction progress (expressed as mass of fuel dissolved per solution volume) of more than four orders of magnitude was covered. By dissolving mm sized fragments in large volumes of solution, saturation effects were avoided and intrinsic fuel matrix dissolution rates of 0.3% of the inventory per year were measured, corresponding to upper limits of surface area normalized rates of about 5-20 mg/(m^2d). Surface area normalized reaction rates were significantly lower when using fine grained fuel powder (estimated sample surface area to solution volume ratio (S/V) ca. 3000 m^{-1}), however, no decrease of reaction rate with time was observed. The dependency of reaction rates on S/V may be rationalized by radiolysis effects.

The pH in the solutions during the progress of the reaction remained neutral to slightly alkaline. Eh values are significantly reduced with respect to air saturated waters. Eh values are lower in tests using NaCl solutions than in tests using deionized water as a leachant. Highest pH values (9.6) and lowest Eh values (<-300mV) were measured in the presence of iron as an additive to the corrosion test. No acidifying or oxidizing effect by radiolysis on the solution pH and Eh values was observed. The formation of the radiolysis gases oxygen and hydrogen was observed, in quantities proportional to the spent fuel sample mass, independently on the surface area of the sample. We conclude that the radiolysis gases are produced by gamma- and not by alpha radiation. In the presence of iron, no oxygen was observed in the gas phase, indicating that oxygen uptake by iron corrosion effectively removes oxygen formed by radiolysis.

The ratios of the various isotopes of U, Pu, Cs and Eu found in solution and of Xe and Kr in gas phase match the average isotopic ratios in the fuel. Sr90 release data were found to

be useful in indicating the kinetics of the degradation of the fuel matrix. Release of Tc99, Np237 and Sb125 occured with a similar rate than that of Sr, hence, release of these elements is controlled by the kinetics of the degradation (oxidation, dissolution) of the fuel matrix. Preferential release of Cs134/137 was observed, representing release from grain boundaries. Even at low reaction progress values (experiments with single mm sized fragments in large solution volumes) the solution concentrations of U, Pu238/239/240/241/242, Am241, and REE were significantly lower than anticipated from the extend of fuel matrix dissolution. Concentrations are controlled by a combination of sorption, precipitation and coprecipitation phenomena. The maximum concentrations of Pu and U in the tests are close to reported solubility limited concentrations in pure 5m NaCl solutions, whereas Am concentrations remain five orders of magnitude lower than the solubility limit of the expected stable phase $Am(OH)_3$.

The presence of iron effectively reduces the solution concentration of almost all measured radionuclides.

The dissolution of **unirradiated UO_2** has been studied under similar conditions as those of the spent fuel tests. The corrosion behavior of unirradiated UO_2 in a NaCl-rich brine has been studied also as a function of oxygen partial pressure. Under reducing conditions initially a rapid increase in the solution concentration of uranium was observed, followed by a decrease. This decrease was attributed to the precipitation of U(IV)-hydroxide. Finally constant U-concentrations were achieved. The final value agrees with the solubility of UO_2 as determined in 5 m NaCl - solutions at the same conditions. Under oxidizing conditions dissolution rates were measured in a replenishment test. The oxidation state of the surface was analysed by XPS. Three stages were distinguished: (1) fast dissolution of an oxidized surface layer with a composition of $UO_{2.6}$; (2) slow dissolution uranium dioxide and formation of a stationary surface film of $UO_{2.4}$ (3) dissolution after replenishment. Similar rates before and after replenishment are explained by the fact that the oxidation state of the dissolving surface before and after replenishment is the same. XPS analyses resulted in a surface composition of $UO_{2,4}$, which is close to that, obtained in dissolution tests with diluted solutions. This might be an indication, that the dissolution mechanism of UO_2 in brines and diluted solutions is similar. Under anoxic conditions reaction rates were significant lower than under oxidizing conditions..

1 CORROSION TESTS WITH SPENT FUEL.

Our work aims at characterizing and qualifying the chemical durability of unprocessed high burnup UO_2 fuel as waste form for disposal sites in salt formations. The chemical stability is commonly assessed by performing leach (corrosion) tests and subsequent sample surface and solution analyses. Surface analyses by XPS have shown that under oxidizing and anaerobic conditions, the dissolution process of the UO_2 matrix and the associated radionuclide release is preceeded by surface oxidation to U_3O_7 or U_4O_9 [Johnson and Shoesmith, 1988, see also results of solubility tests with unirradiated UO_2, second part of this report]. It is rather difficult to deduce from analyses of leach solutions the processes which control fuel alteration, because radionuclides are transferred to the aqueous phase simultaneously from the UO_2-matrix, from grain boundaries, from the fuel/sheath gap and fracture surfaces, from segregated phases and from the cladding and, subsequently, the nuclides may become immobilized again in secondary phases or be sorbed on solid surfaces. Using powdered fuel samples, Gray et al. [1991, 1993] succeeded recently in distinguishing matrix dissolution effects from other effects. Avoiding saturation effects under oxidizing conditions by using leach tests with fast flowing water, they obtained matrix dissolution rates of about 1 to 5 mg/(m^2d) at 25°C. The rate limiting process and potential saturation (steady state or solubility) effects are not yet known.

Using static tests with very different dimensions and consequently different surface area to solution volume ratios (S/V), we want to distinguish between solubility, inventory and rate controls for releases of radionuclides. An overview on the actually running spent fuel corrosion tests at 25°C is given in Table I. Tests at 150°C were started. The behavior of a large quantity of radionuclides is analysed in order to identify general corrosion properties of the fuel matrix and element specific secondary processes. Eventually, the results will allow extrapolation of laboratory data to a realistic hydrogeologic situation in a repository. Unambiguous interpretation of all results is not yet possible as the surfaces of the samples, the zircalloy claddings and the reaction vessel will only be characterized at test termination.

Table 1: Overview on actually running spent fuel corrosion tests at 25°C (Dec. 1993)

Sample	Mass (g)	Solution	Wash cycles(d)		Corrosion tests under static conditions						
			Duration (d) of		Accumulated corrosion time (d) and dates of sampling solution (S 1 - S 5);						
			Cycle 1	Cycle 2	S 1	S 2	S 3	sampling of gas	S 4	S 5	Code
*K 1	7,335	DI-Water	31	45	45	107	199	418	437	running	WDOA 1
K 2	7,109	DI-Water	31	45	45	107	199	418	437	running	WDOA 2
K 3	6,976	NaCl - sol.	30	41	a) 52	114	206	344	438	running	NDRA 1
K 4	7,534	NaCl - sol.	31	42	b) 50	112	207	284	438	running	NDRA 2
K 9	7,429	NaCl - sol.	31	42	53	116	207	390	441	running	NDOA 1
K 10	7,369	NaCl - sol.	32	42	52	115	206	390	442	running	NDOA 2
**F 3	0,02	NaCl - sol.	33	43	49	112	203	n.m.	437	running	NFOA 1
F 4	0,008	NaCl - sol.	33	43	49	112	203	n.m.	440	running	NFOA 2
***P 1	2,9	NaCl - sol.		42	c) 40	83	201	385	409	running	NPOA 1
P 2	2,95	NaCl - sol.		42	d) 42	83	201	385	409	running	NPOA 2

*K: compact pellet with cladding
**F: fragment
***P: powder (O< 5μm)

Addition of:
a) 8,5 g Fe-powder (Ø < 10 μm)
b) 9,5 g Fe-powder (Ø < 10 μm)
c) 0,65 g Zircaloy - cladding
d) 0,65 g Zircaloy - cladding

1.1 GENERAL PREPARATIONS; ANALYTICAL TECHNIQUES AND SAMPLE PREPARATIONS.

1.1.1 EXPERIMENTAL

The experimental procedure is only briefly summarized and analytical procedures are updated. Details can be found in the annual report of 1992. The spent fuel rod SBS1108 used in our experiments was obtained from SIEMENS/KWU. It is UO_2 fuel of 3.8% initial enrichment, discharged May 1989 after a total irradiation time of 1226 days from the PWR-Gösgen/Switzerland with an average linear power of 260 W/cm (max. 315 W/cm) and a high burnup of 50.4 MWd/kgU. The initial fuel/sheath gap was 170 μm and the specific activity 7.4 10^{10} Bq/g (Feb. 1992).

Sample preparations

We prepared three types of samples with the aim to cover large differences in the effective surface area: compact pellet sized fuel segments (ca. 7 g each), cut from the fuel rod, individual fuel fragments (ca. 10 mg each), selected after coarse sieving and powdered fuel (grain size 3 μm, 2.9 g). Powders were prepared from fuel pellets using a ball mill. The appropriate size fraction was obtained by dry sieving with the help of 10 agate balls (1cm diameter). Powders were cleaned from adhering fines by 2 times ultrasonic treatment in NaCl solutions, 10 min each. The wash solutions were analysed for radionuclide contents. Sample preparation, transportation and storage were performed under N_2 atmosphere.

Test description

Tantalum lined autoclaves were used as reaction vessels (volume: 500 mL), in order to minimize reactions between agressive salt solutions and container walls. Upon contact to aqueous media, Ta forms a thin oxide film (ca 2 nm) which is impermeable to hydrogen and does not react with acid or slightly alkaline salt solutions. The lid of the autoclave was equipped with two ball valves (Ti). Experiments are performed under static conditions in 200 mL 95% halite (NaCl) saturated, anaerobic (Ar), carbonate free solutions at 25°C. Cladding was present in tests with pellets and with fuel powders. Prior to static testing, the samples were "washed" twice in NaCl solution under Ar-atmosphere, for periods each of one month duration, to remove the gap inventory of Cs and possibly oxidized surface layers. Thereafter, the experiments were continued under static conditions. In two tests 7 g iron powder (Merck 3819, average grain size 10 μm) were inserted after starting the static test. The leachates were sampled periodically by means of a syringe passing through one of the two ball valves in the lid of the autoclave. During sampling, water saturated Ar is flushed through the other valve,

thus avoiding air contamination.

Sample surface to solution volume ratios (S/V) in the tests

The surface area of the fuel samples used is not known exactly but minimum values may be estimated from geometrical considerations. Due to surface roughness, effective surface areas may be 2-3 times higher and effective surface areas may be further increased by water accessible grain boundaries. With a typical fragment diameter of about 2-3 mm, the specific surface area of a fractured pellet is at least 2 cm^2/g (fragments idealized as cubes) corresponding to 14 cm^2 surface area of a pellet sized fuel segment. However, if only the two cross sections of the segment are considered exposed to the solution, the effective surface area may be as low as 1.3 cm^2. The individual fragments used have a diameter of about 1mm, corresponding to a specific surface area of at least 7 cm^2/g and a sample surface area larger than 0.06 cm^2. Even if we can only estimate the absolute effective surface area, we know in relative terms that the surface area of an individual fragment is about 200 times smaller than that of a fractured pellet. For the powdered fuel with an average grain diameter of about 3 µm the specific surface area is about 3000 cm^2/g and the sample surface area is 8700 cm^2. Considering these assumptions, the sample surface area to solution volume ratio (S/V) was varied by many orders of magnitude. It is >3000 m^{-1} for powders, >20 m^{-1} or 2 m^{-1} for pellets, and >0.01 m^{-1} for fragments.

Gas analyses

Using an evacuated (10^{-6} mbar) gas collection cylinder (V=50 cm^3), the atmosphere inside of the reaction vessels was sampled. Gas composition was analysed quantitatively by a quadrupole mass spectrometer (GAM 445, Balzers, Lichtenstein). Calibration was performed, using a gas mixture of known amouts of H_2, N_2 O_2, Kr and Xe in Ne.

Eh/pH analyses

In order to avoid air contamination (oxidation, CO_2-uptake) Eh and pH values were determined only few minutes after solution sampling. Measurements were performed under N_2-Atmosphere inside the hot cell. In case of NaCl solutions, measured pH data were corrected for liquid junction potential. Liquid junction potentials were obtained by measuring the pH value of 95% saturated NaCl solutions of known activity a_{H+}. Reported pH values are consistent with Pitzer's pH convention (ionic splitting convention).

Details of the radiochemical separation and analyses procedure

Solution samples were filtered through 0,45 μm filters in order to remove fuel particles. An aliquot of some samples was passed further through an ultrafiltration membrane (pore size 18 A) to check for colloid formation. Most of the radionuclides analysed in solutions could only be determined after radiochemical separation. In order to get a feeling for the reliability of the analytical procedure the quality of the applied methods has been validated, where possible, by internal standardisation using isotopic tracers and additionally by intercomparison runs with the radiochemical laboratory of the institute of hot chemistry (IHCH). A flowsheet of the analytical steps is shown in fig. 1.

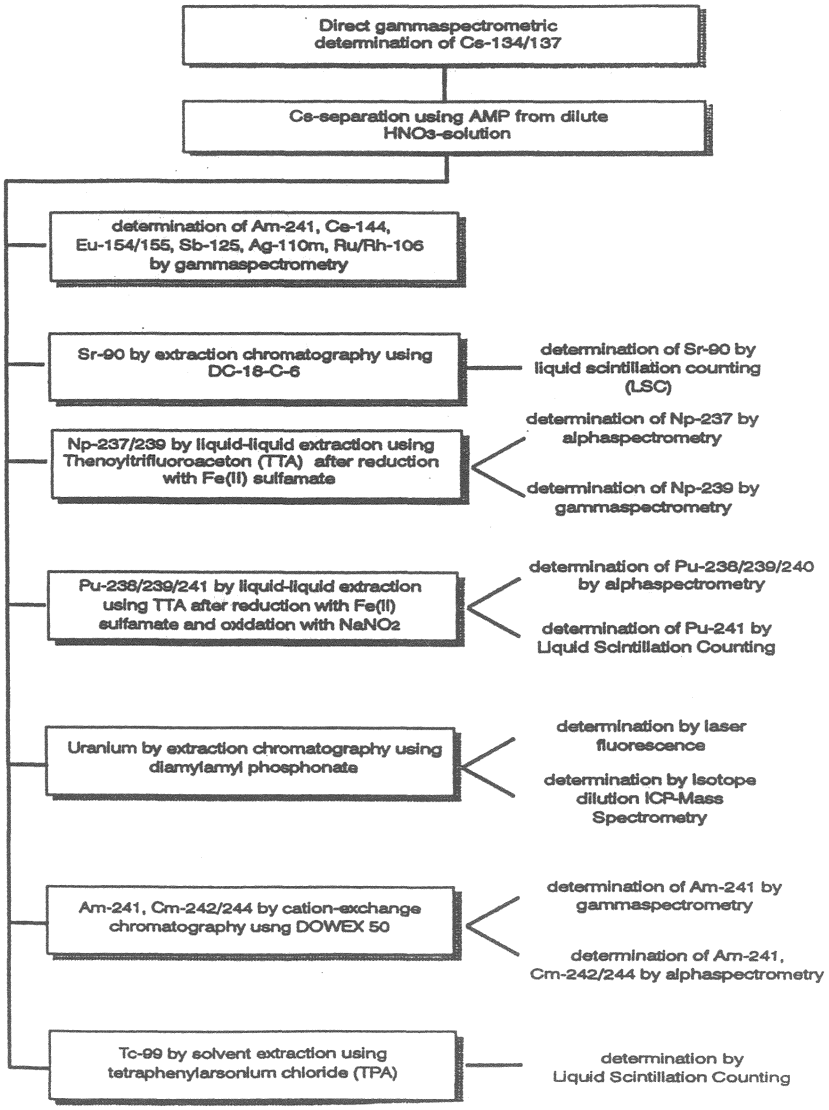

Fig.1 Flowsheet of the radioanalytical procedure

Only Cs-134 and Cs-137 were determined directly by γ-spectrometry in diluted sample solutions (dilution factor: 1000). Other γ-emitting nuclides such as Am-241, Ce-144, Eu-154, Eu-155, Ru-106, Ag-110m and Sb-125 could be detected after separation of the Cs-isotopes being present in high excess. Cs is removed by specific sorption on the inorganic cation-

exchanger ammonium molybdophosphate (AMP). Due to the high γ-doserate of some sample solutions the separation is carried out by adding 3 g AMP to 10 ml of the 1:10 diluted solution in a shielded alpha-box with remote handling. Cs is effectively removed from solution with decontamination factors of about 10^3-10^4. After filtration through a membrane filter with pore diameters of 0,45 µm, all other radionuclides were determined subsequently in the filtrate. Recovery rates for other nuclides after Cs-separation in the filtrate were determined to range from 95 to 100 %.

Due to the Cs-separation the Compton-background of the γ-spectrum decreased to such an extent, that other γ-emitting isotopes like Ce-144, Eu-154/155, Am-241, Sb-125, Ag-110m and Ru-106/Rh-106 could be detected. γ-spectra of a sample solution before and after Cs-separation are shown in fig.2.

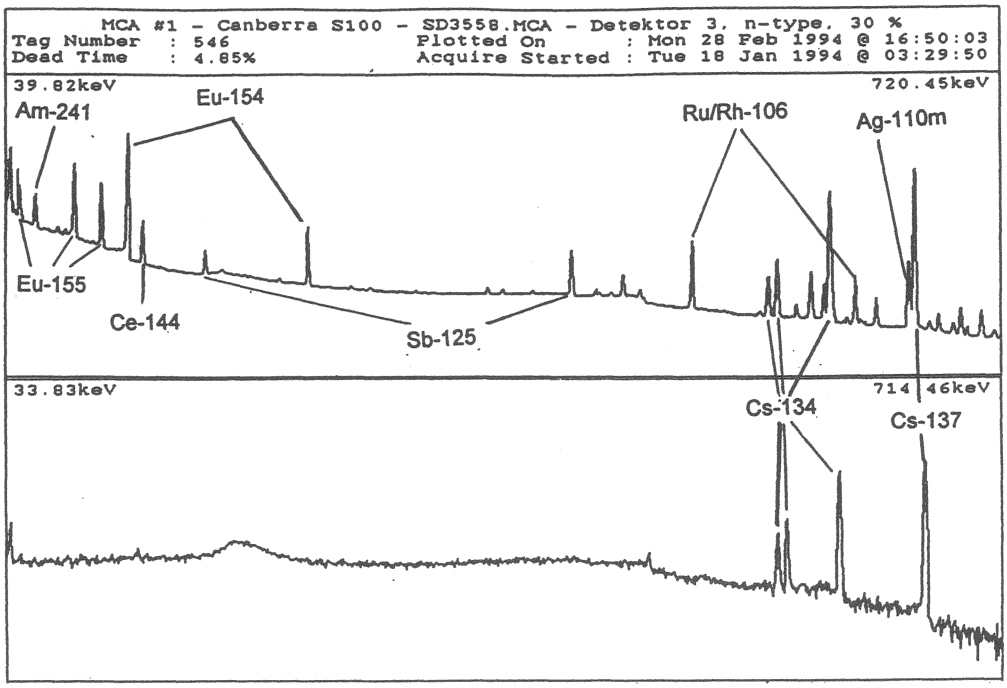

Fig.2 γ-spectra of the same sample solution before (lower spectrum) and after (upper spectrum) Cs-separation

The radiochemical separation of Sr-90 is carried out using a chromatographic material consisting of an inert support and di-tert-butyl-cyclohexyl-18-crown-6 as a selective extractant for Sr. A 1ml aliquot of the sample solution after Cs-separation, adjusted to 8 M HNO_3 and after addition of non-radioactive Sr-tracer, was passed through a 1 ml column. Sr eluted with 10 ml 0,05 M HNO_3 and an aliquot of the eluate was measured immediately by LSC. The result of this measurement is verified by a second LSC-analysis after ingrowth of the daughter nuclide Y-90. Thus, it is possible to eliminate errors due to other co-extracted

radionuclides. The separation yields, which were determined by ICP-AES-analysis of the non-radioactive Sr added as a tracer varied between 83% to 93%. Care had to be taken for cross-contamination effects from one sample to another, due to a slow kinetic of the Sr-desorption from the column. Therefore it has been necessary to wash the column after and before each separation extensively.

Tc-99 as TcO_4^- forms ion pair complexes with tetraphenylarsonium (TPA) and then can be extracted into $CHCl_3$. The sample aliquot had to be adjusted to 0,5 M HNO_3 and then was mixed with a solution of TPA chloride in $CHCl_3$. Tc-99 in the organic phase was directly analysed by LSC. Interferences due to low amounts of co-extracted Ru/Rh-106 can be minimized by an appropriate window setting in the LSC-spectrum.

1 ml aliquots of the sample solution were submitted to solvent-extraction using thenoyltrifluoracetone (TTA) for the separation of Np and Pu. A selective extraction of both elements separately is possible by adjusting different oxidation states. Firstly Np was reduced from V to IV using Fe(II)sulfamat and then was extracted by TTA from 1 M HNO_3, while Pu, existing in oxidation state (III), was not. After washing the organic phase and stripping to 8 M HNO_3, the aqueous solution is evaporated on a stainless steel dish and analysed by α-spectrometry. In a second aliquot of the solution Pu was reoxidized to its oxidation state (IV) with $NaNO_2$ after the reduction step. After re-extraction of Pu into 8 M HNO_3-solution Pu-238 and Pu-239/240 were determined by α-spectrometry and Pu-241 by LSC. The separation yield for the Pu-separation was taken into consideration by using Pu-236 as an isotopic tracer. It was found that NaCl-concentrations have almost no influence on the Pu-extraction yield until 2 M (fig.3).

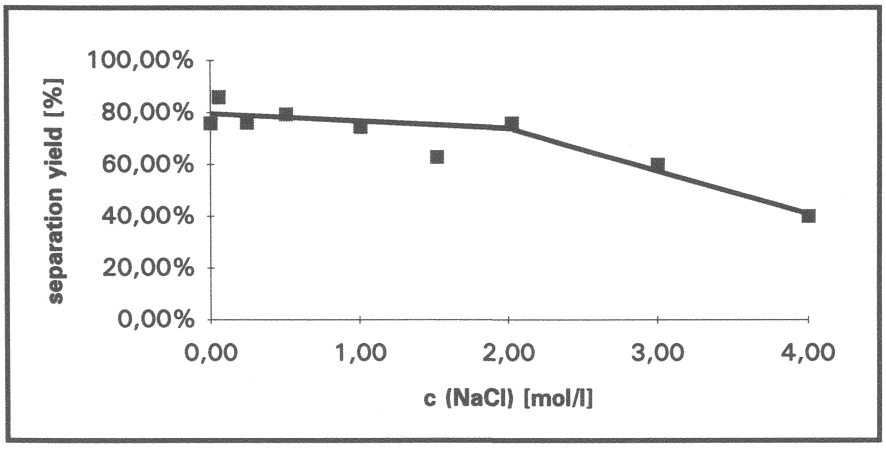

Fig. 3 Separation yield of Pu-extraction by 0,5 M TTA in xylole from 1 M HNO_3 and different NaCl content of the aqueous phase

Am-241 and Cm-242/244 were separated from 1 M HNO_3-solution by cation-exchange chromatography using DOWEX 50Wx8. After washing the column with 1 and 2 M HNO_3, the trivalent actinides were eluted with 6 M HNO_3 and determined by alphaspectrometry.

The analysis of uranium was not possible by radiometric methods, due to the low specific activity of the uranium isotopes and low concentrations in sample solutions. Therefore two methods - a compact laser fluorescence spectrometer (LFS) (SCINTREX, UA-3) and ICP-mass spectrometry (ICP-MS, Perkin-Elmer) - have been tested for their suitability of uranium trace analysis. For both methods it is necessary to separate uranium from an excess of matrix components. Especially in the case of LFS, uranium fluorescence is heavily influenced even by low salt or acid concentrations. Uranium separation has been carried out in 3 M HNO_3-solution by extraction chromatography using diamyl amylphosphonate sorbed on an inert support. For LFS-analysis uranium is desorbed from the column by a buffer containing 0,5 M H_3PO_4/0,04 M $Na_4P_2O_7$. The phosphate/pyrophosphate buffer additionaly serves as a fluorescence amplifier. After neutralisation of the acidic solution the sample was filled into a quartz cuvette and fluorescence intensity was measured. The uranium concentration was quantified by the standard addition method. From the 3 σ-error of the background a detection limit of 0.6 ppb was calculated.

ICP-MS offers two advantages over LFS:

- isotope dilution analysis can be applied using U-233 as tracer
- isotope ratios of uranium can be determined

After addition of U-233 as an isotopic tracer the separation from the matrix was done as described before. With 0.5 M $H_2C_2O_4$ uranium was eluted and the solution directly submitted to ICP-MS analysis. As detection limit 0,01 ppb was calculated for the analytical conditions used, thus being one order of magnitude lower than LFS. Separation yields varied from 92 to 100 %. Fig. 4 shows a comparison of uranium concentration measured by LFS and ICP-MS.

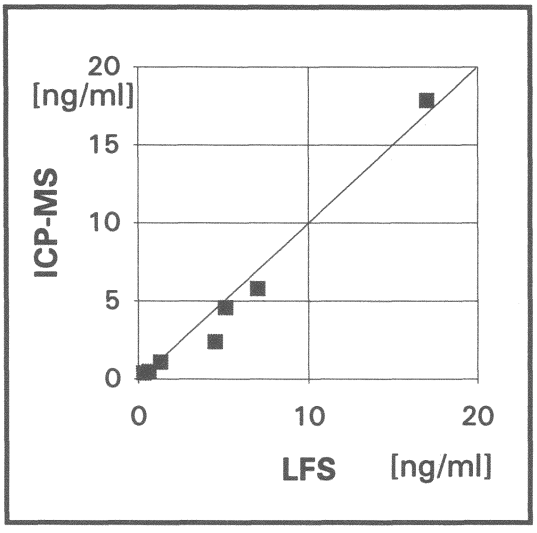

Fig. 4 Comparison of uranium concentrations determined by laser fluorescence and ICP-MS after chemical separation of uranium

Considering the low uranium concentrations in the lower ppb range the conformity of the results is quite satisfactory. Due to the lower sensitivity of ICP-MS against matrix effects and the possibilities to apply isotope dilution analysis and to determine isotope ratios the latter method was favoured over LFS analysis.

Analytical quality control

In order to guarantee a high confidence level in the analytical results two kinds of quality control methods were applied:

- internal quality control

For most of the radiochemical separations isotopic tracers were added to the sample solution in order to verify the chemical yield of the whole procedure. This has been done for Sr-analysis using non-radioactive Sr, for Pu-analysis using Pu-236 and for U-analysis using U-233.

Pu-analysis was checked for plausibility by comparing the total α-activity of all Pu-isotopes determined by α-spectrometry with gross α-activity measured by LSC (fig. 5).

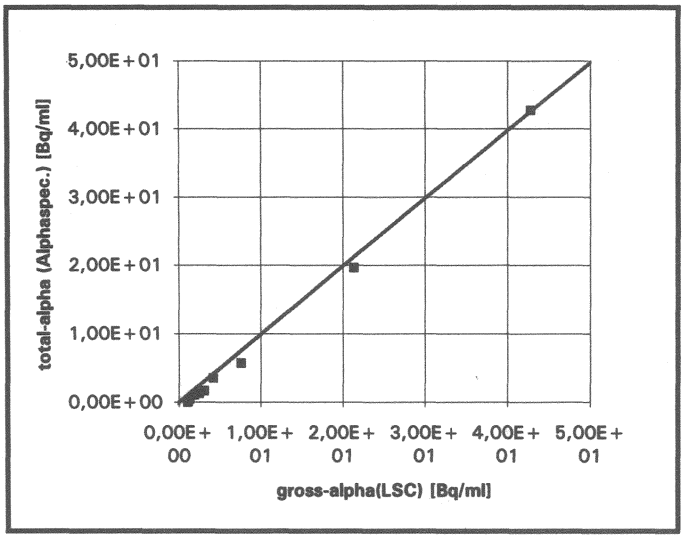

Fig. 5 Quality control of Pu-analysis by comparison of total α-activity determined by α-spectrometry with gross-α-activity determined by LSC

Am-241 analysis was additionally verified by comparing direct γ-measurement after Cs-separation and determination after cation-exchange separation of the trivalent actinides and alphaspectrometric analysis.

- external quality control

An intercomparison was organized with the radioanalytical laboratory of IHCH. As an example the results of Pu-238 analysis, Sr-90-analysis and determination of Am-241 were compared in fig.6. In general the results agree satisfactorily and show scattering only in the lower concentration range, thus demonstrating the limits of the analytical methods.

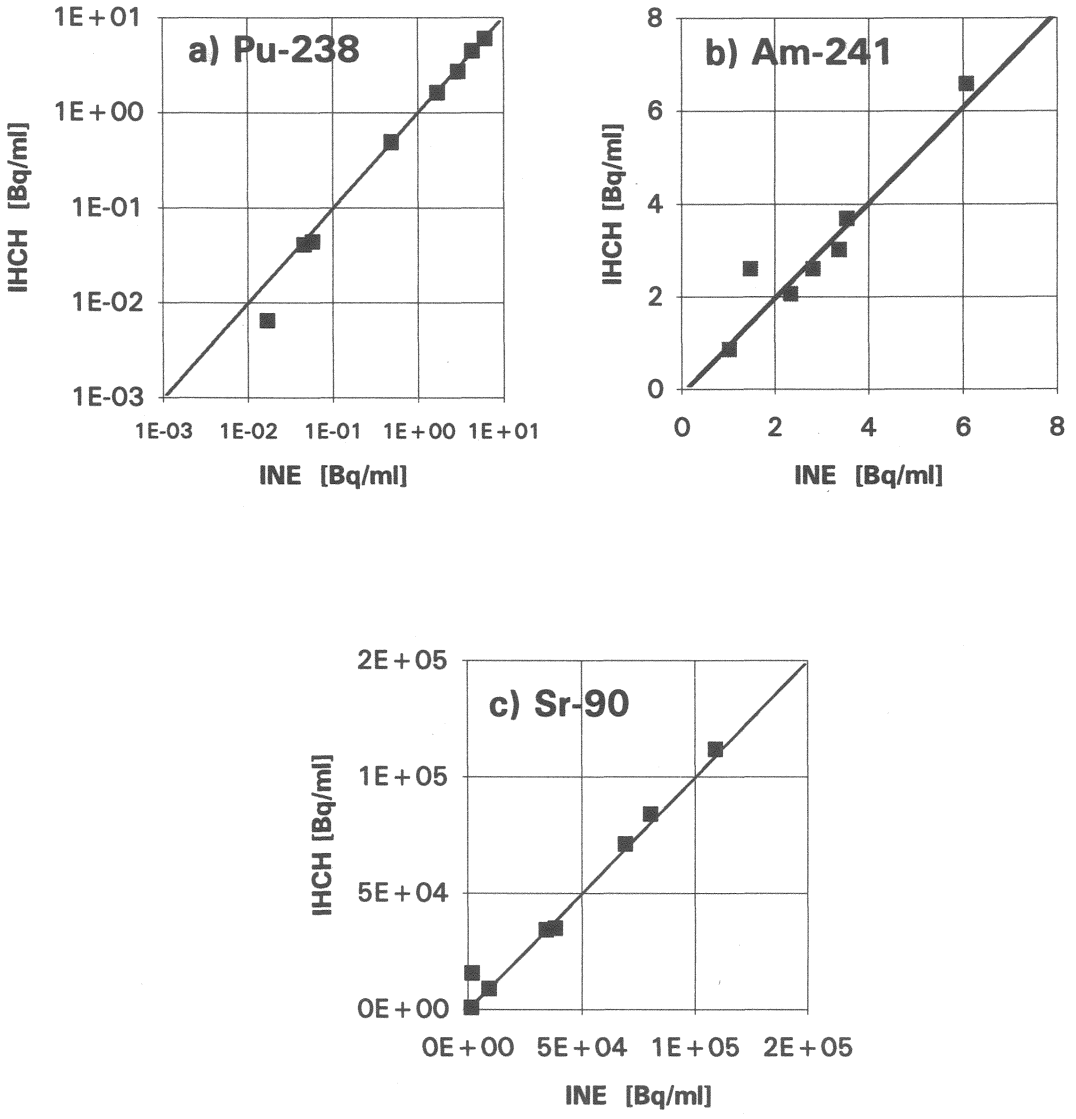

Fig. 6 Intercomparison test run for the determination of a) Pu-238, b) Am-241 and c) Sr-90 after radiochemical separation methods by INE and IHCH laboratory

1.1.2 RADIONUCLIDE INVENTORY IN THE FUEL

Description of inventory measurement techniques

Nuclide inventories of the fuel samples were both measured and calculated with the help of the KORRIGEN code [Fischer and Wiese 1983, Version 1990] using a neutron cross section library applicable to high burnup values. KORRIGEN results are reported in the last annual report. However, the exact knowledge of the inventory is of high importance, when calculating release rates and concentrations of radionuclides in corrosion solutions. In order to obtain exact values of the radionuclide inventory of spent fuel and in order to determine the degree of homogenity of the radionuclide distribution, small fragments from defined locations, as central part, rim or cladding were selected, dissolved and then analyzed radiochemically.

Sample preparation.

For preparation, a disc, 5 mm in height was cut from a pellet by means of a diamond saw. A fragment was selected from the centre and another one from the rim of the fuel pellet, each about a few millimeters in size. A part of the zircaloy cladding was dissolved in order to analyze the composition of adhering fuel grains and potentially segregated phases.

Dissolution process.

The complete dissolution of high burnup spent fuel samples requires much more efforts than for "normal" and low burnup spent fuel. The specimen were dissolved by boiling them in a mixture of 13 m HCl and 14 m HNO3 ("Königswasser") for 20 or 135 minutes, respectively. Weights of the dissolved spent fuel samples and dissolution acids are listed below.

	"Rim"	"Centre"	"Cladding"
Sample	0,119 g	0,133 g	0,826 g (mainly ZrO2)
13 m HCl	8,84 g	9,27 g	25,201 g
14 m HNO3	3,68 g	3,98 g	11,114 g
Boiling time	20 minutes	20 minutes	135 minutes

From the resulting solutions aliquots were taken and diluted (1:100) with 1 m HNO3. The radionuclide composition of the solutions was performed by radiochemical analytical methods as described in the annual report 1992

Results

The specific activities of the particles from the center and the rim, obtained after preceeding dissolution are listed in Table II, together with the specific activities, as calculated by the KORIGEN code, related to the reference date February 1st, 1994. In Figure 7 the specific activities of the radionuclides analyzed are plotted together with the calculated data. As shown in Figure A and Table A, the deviation of the analysed activties from the KORIGEN data is in general not very high. Slightly higher specific activities were determined for Cs-134, Cs-137, Sr-90, Tc99, Am-241, Am-243, Np-239, Cm-244, Cm-242, Pu-238, Pu-239/40 and slighly lower specific activities were found for Eu-154, Sb-125 and Ag-110m, in comparison with the KORIGEN data. The good agreement between center and rim data indicate that radionuclides are distributed rather homogeneously radially in the fuel. The often reported "rim effect" of higher burnup and higher nuclide concentrations in the outer part of the rim (100 μm) was not observed, probably because the rim sample was larger than a mm in diameter. Hence, the radionuclide inventory of this fuel sample is controlled by the bulk part of the fuel. The rim effect may be studied by analyzing the fuel adhering to the cladding.

The specific radionuclide activities of the fuel grains adhering to the interior of the cladding cannot be calculated from the activity in solution after dissolution, because the weight of the grains is unknown. In order to allow a comparison between the radionuclide activities of this material and those of the samples from the centre and the rim, the measured nuclide activities were normalized to the Sr-90 activity. The result is given in Figure 8 as the activity ratios of the measured radionuclides to Sr90.

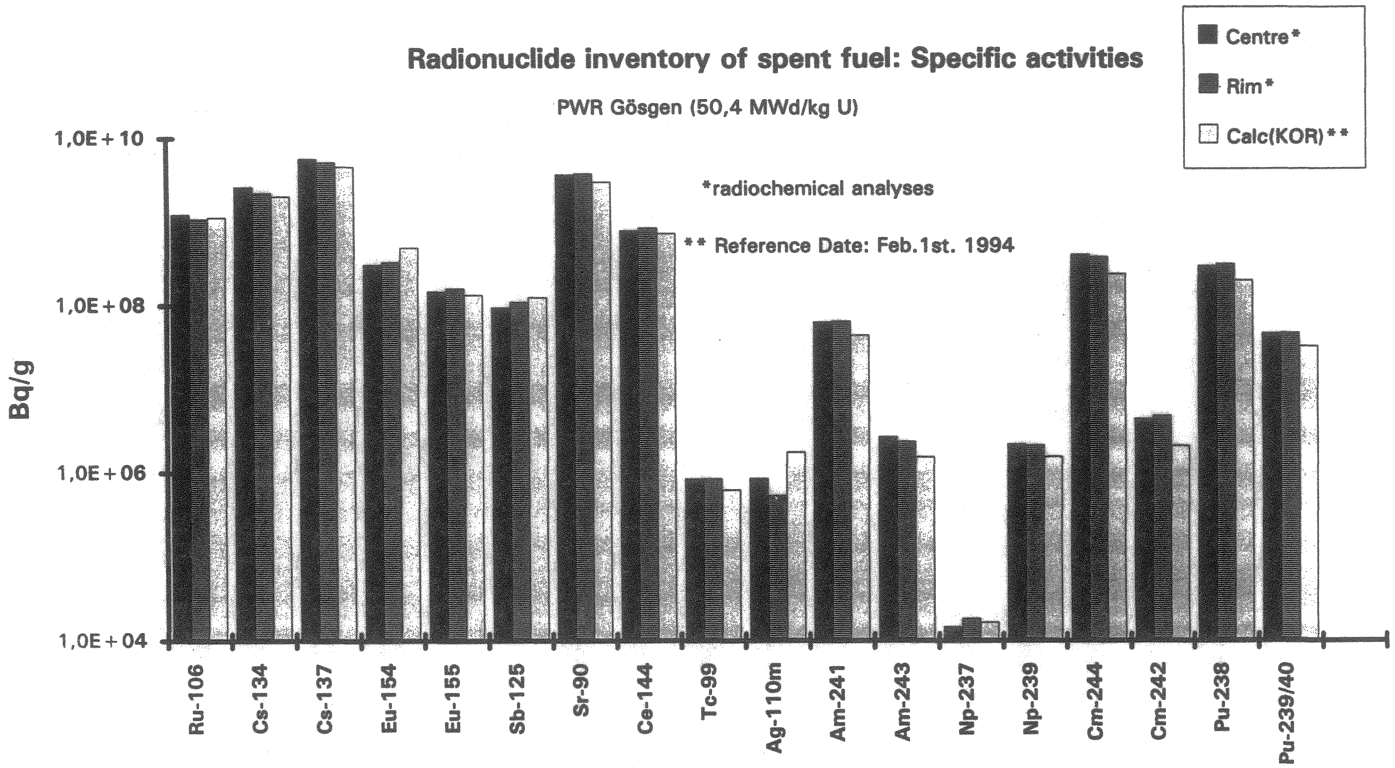

Figure 7: Specific activities of radionuclides in spent fuel samples at different radial positions (center and rim), measured after preceeding dissolution in comparison with inventory data, calculated by the KORIGEN computer code.

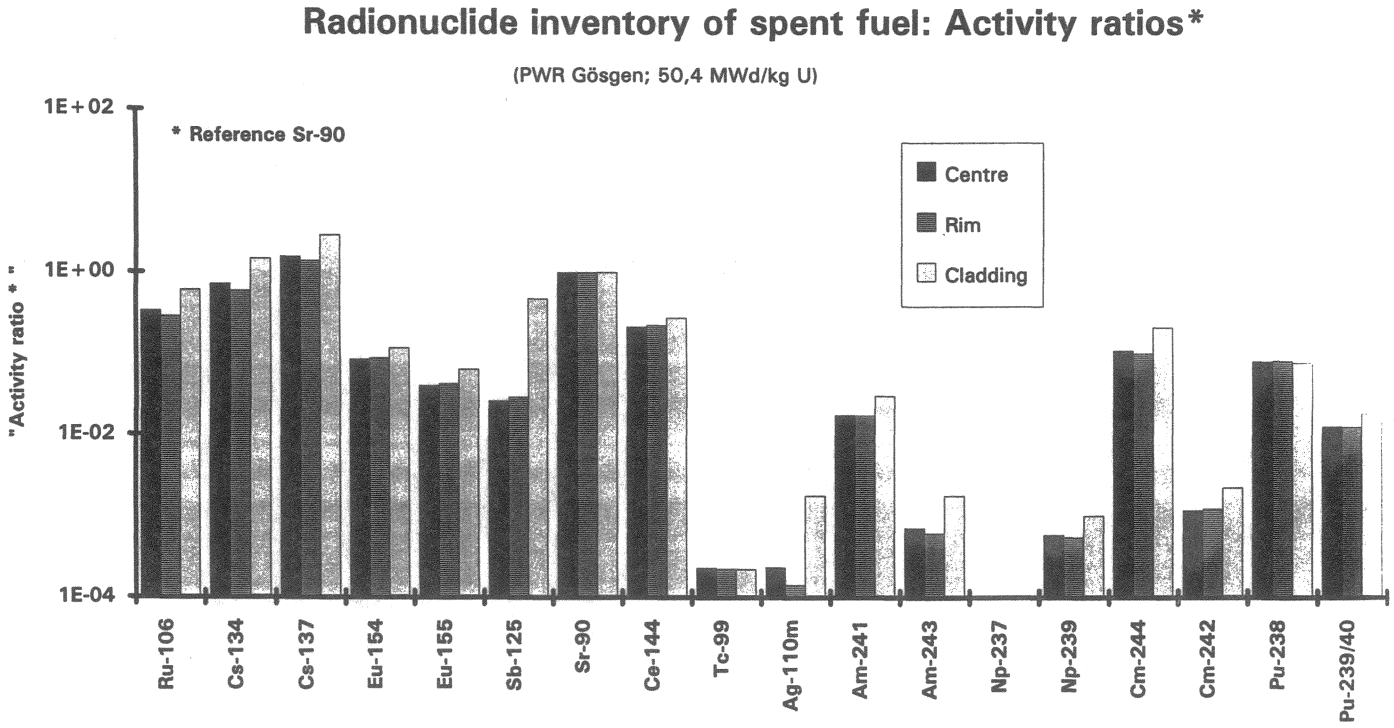

Figure 8: Activity ratios of radionuclides (reference Sr-90) at different radial positions in spent fuel samples, measured after preceeding dissolution.

Table II: Analyzed and calculated specific activities of high burnup spent fuel from PWR-Gösgen (* Data are related to Febr.1st,1994).

Nuclide	Centre Bq/g	Rim Bq/g	Calc (KOR) Bq/g HM
Ru-106	1,22E+09	1,08E+09	1,13E+09
Cs-134	2,62E+09	2,22E+09	2,02E+09
Cs-137	5,71E+09	5,21E+09	4,58E+09
Eu-154	3,09E+08	3,30E+08	4,91E+08
Eu-155	1,47E+08	1,60E+08	1,34E+08
Sb-125	9,47E+07	1,09E+08	1,25E+08
Sr-90	3,66E+09	3,78E+09	3,00E+09
Ce-144	7,81E+08	8,38E+08	7,22E+08
Tc-99	8.54E+05	8.54E+05	6,29E+05
Ag-110m	8,63E+05	5,40E+05	1,75E+06
Am-241	6,37E+07	6,50E+07	4,38E+07
Am-243	2,65E+06	2,35E+06	1,54E+06
Np-237	1,48E+04	1,85E+04	1,65E+04
Np-239	2,17E+06	2,10E+06	1,54E+06
Cm-244	4,01E+08	3,78E+08	2,36E+08
Cm-242	4,37E+06	4,70E+06	2,07E+06
Pu-238	2,94E+08	3,09E+08	1,97E+08
Pu239/40	4,63E+07	4,70E+07	3,23E+07

1.2 CHARACTERIZATION OF THE DURABILITY OF SPENT UO_2 FUEL IN SATURATED NACL BRINES

The corrosion behavior of the fuel and associated mobilization of radionuclides is deduced mainly from radiochemical solution analyses. Radionuclide mobility is assessed (1) in relative terms by calculating from the measured radioactivities the fraction of the nuclide inventory of a fuel sample found in the aqueous phase (FIAP) and (2) by calculating elemental solution concentrations. The extent of matrix dissolution may be expressed as "normalized mass loss, NL_i" of the nuclide i. This unit is frequently used to describe the dissolution behavior of nuclear waste borosilicate glass. If the NL_i values of uranium and of the nuclide i are the same, than the nuclide i is released congruently with the dissolution of the matrix. NL values were calculated from FIAP values, using the estimated minimal geometric sample surface areas S and the sample mass m.

$$NL_i = FIAP_i * m/S$$

Using the formula

$$d_i = NL_i/\rho$$

with the density ρ of the fuel (10.4 g/cm^3) one obtains a depth d_i from which the nuclide i is released. In case of glass this depth is known as a "depletion depth". NL and d values are upper limits as the effective surface area is probably higher than the geometric.

Gas phase

The fission gases Xe and Kr were measured in isotopic ratios which match predictions by the KORRIGEN code. H_2 gas was detected in all experiments, resulting from radiolysis and in the presence of iron additionally from the corrosion of iron. Radiolytic H_2 production is directly proportional to fuel sample mass and independent on the sample geometry. In a half year 2.9 g of powder generated ca. 3 Vol% H_2 whereas. 7 g pellets generated 7 Vol% H_2 in 200 mL gas volume of ca.1 atm). This finding may help to distinguish between alpha- and gamma-radiolysis. As the escape depth of alpha-particles out of the fuel is limited to few µm, one would expect much higher specific H_2-production for powdered fuel samples than for fuel pellets, if H_2 radiolysis resulted mainly from alpha-radiolysis. This is not the case and we may use this as an indication that mainly gamma-radiolysis is responsible for H_2-formation. About 30% less H_2 was produced in the experiments using deionized water when compared to NaCl solutions. Only traces of N_2 (<0.2 Vol%) where observed in the reaction vessel, indicating effective sealing of the autoclaves against the hot cell atmosphere. Oxygen contents in experiments with fuel pellets were about 1 Vol%, clearly resulting from radiolysis, because air is absent. The measured partial pressures of Kr and Xe were compared with the fission gas inventories calculated by the KORRIGEN code. In the experiment K4 4%

of the Kr and 6.6% of the Xe inventory were released within 60 days whereas in the experiment K3 the respective numbers are 8% for Kr and 13.7% for Xe after 139 days.

Liquid phase

Eh/pH

The measured data are given in the Eh/pH diagram in Figure 9. This diagram additionally shows the stability fields of water, of various uranium oxide phases and the boundary of FeII/FeIII hydroxides. The pH value remained neutral to slightly alkaline during the tests. Radiolysis obviously does not lead to acidification in nitrogen free chloride media. Eh/pH data for NaCl solutions (samples P1,2, K9,10, F3,4) are located on a line parallel to the stability field boundaries, within the stability field of UO_2. As expected, lowest Eh values are observed in the presence of iron powder. The values are close to the boundary between $Fe(OH)_2$ and $Fe(OH)_3$, indicating that Eh-values may be controlled by this phase boundary. Highest Eh values were observed for the experiments performed in deionized water. This may be rationalized by the lower rates of radiogenic H_2 production in the presence of deionized water (see above).

One should be careful of using our measured Eh values as a measure of the redox state in the corrosion vessels. High simultaneous concentrations of hydrogen and oxygen show that we are dealing with an disequilibrium system (see also that our oxygen measurement data in the Eh/pH diagram differ strongly from the Eh measurements) . Hence the kinetics of redox reactions becomes important. The Eh-electrode (Pt) reacts well with hydrogen, but UO2 reacts much faster with oxygen or even with species such as H_2O_2. Consequently, we may have oxidizing conditions as far as the dissolution of spent fuel is concerned and we have reducing conditions as far as Eh measurement is concerned.

Radionuclide release into the aqueous phase

The cumulative Cs releases ("gap release") from pellet sized fuel/cladding segments and from individual fragments are similar (about 2% of the total inventory), indicating that Cs is homogeneously distributed on all fracture surfaces and solution has penetrated all fractures within the fuel segment. With powdered fuel, all grain boundaries are expected to be exposed to the solution and the major Cs release occurs within few minutes of ultrasonic cleaning. Cumulative release is about 3.5% of the inventory, of which 1.5% (=3.5% - 2% gap inventory) may be attributed to release from grain boundaries.

For the other nuclides the results from dissolution of powdered fuel, a fuel pellet and an individual fragment in 95% saturated NaCl solutions are given in Figs. 10-12 expressed as FIAP-values. Respective data of dissolving a fuel pellet in deionized water are included for comparison (Fig. 14). The released quantities of matrix bound radionuclides Sb125, Eu154, Am241, Pu239/240, Sr90, Ru106 and Ce144 are in most cases between $3*10^{-4}$ and $3*10^{-6}$.

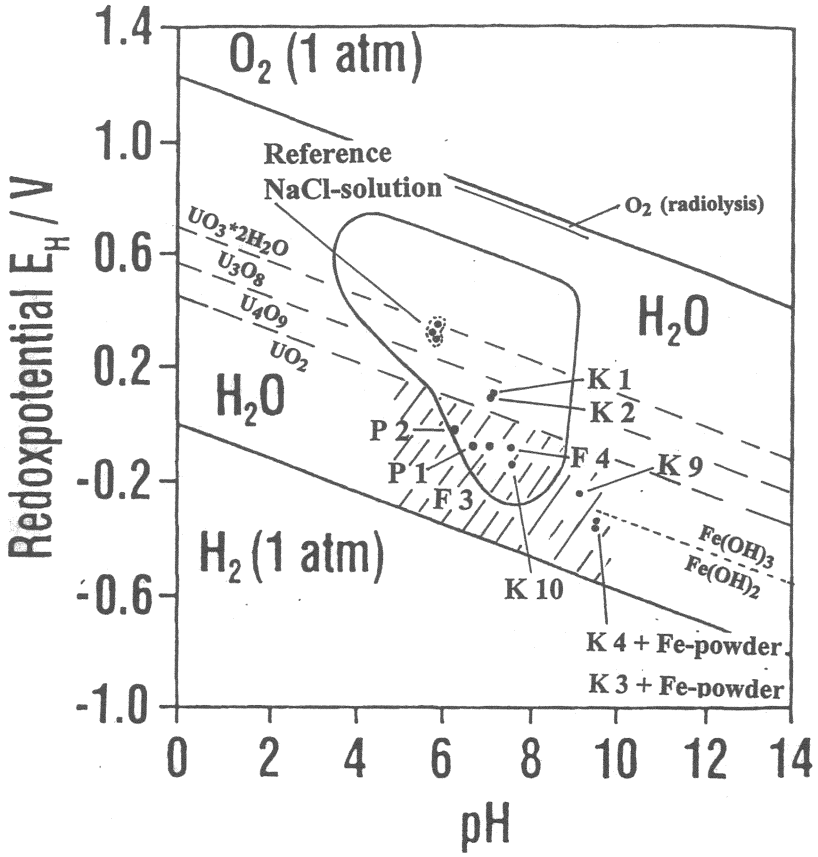

Figure 9 : Diagram of Eh and pH values measured in NaCl-solutions or DI-water contacting KWG spent fuel pellets, powders and -fragments at least for 409 days and in a fresh reference NaCl-solution. Eh/pH values of natural groundwaters from Gorleben are ranging within the enclosed field [Kim 1993]. Additionally, the boundaries of the uranium/oxygen/water -fields are indicated, in accordance to adapted from Garisto [ ]. The shaded area represents the potential - pH region of interest for the UO2 solubility controlled dissolution of spent fuel. The phase boundary $Fe(OH)_2/Fe(OH)_3$ is plotted with reference to [Stumm and Morgan 1981].

Sample name	**State of the samples**	**Corrosion solution**	**Contact time**
K 1, K 2	Pellets	DI - water	437 days
K 3, K 4	Pellets + Fe powder	NaCl-solution (95%)	438 days
K 9, K 10	Pellets	NaCl-solution (95%)	441 days
F 3, F 4	mm-sized fragments	NaCl-solution (95%)	438 days
P 1, P 2	µm-sized powders	NaCl-solution (95%)	409 days

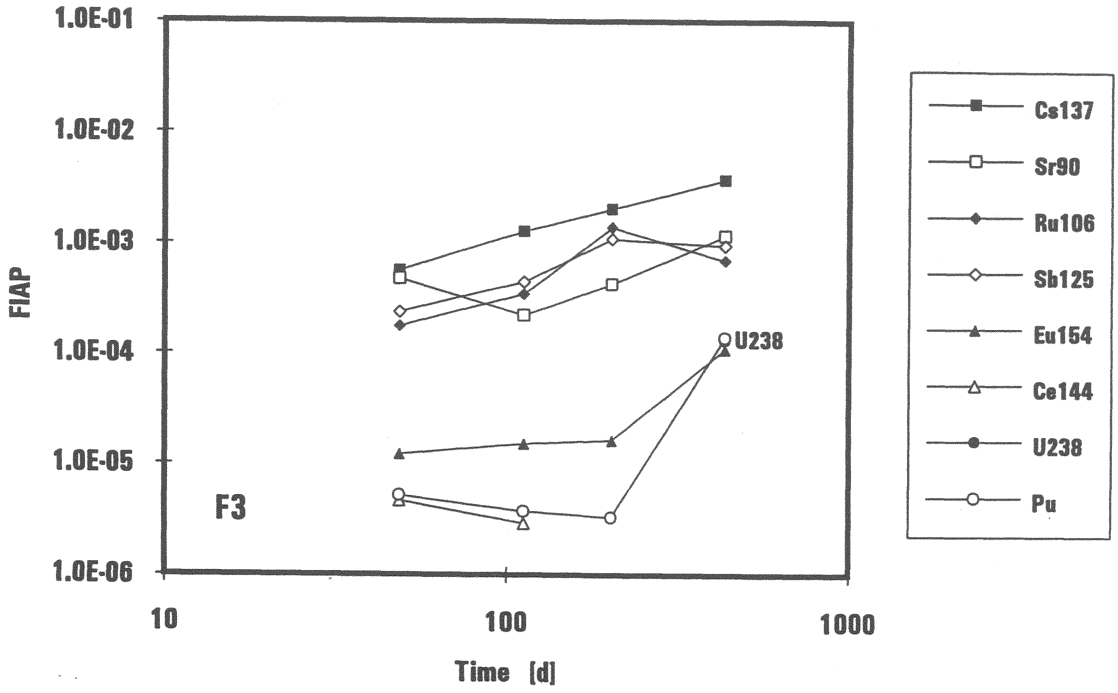

Fig.10. Spent fuel fragment (20 mg) exposed to 200 mL 95% saturated NaCl solution. Fraction of inventories of various radionuclides in the aqueous phase (FIAP) Note: Samples were washed twice in the leachant for periods of 1 month each. Data from wash solutions are not included in the Figures (see annual report 1992)

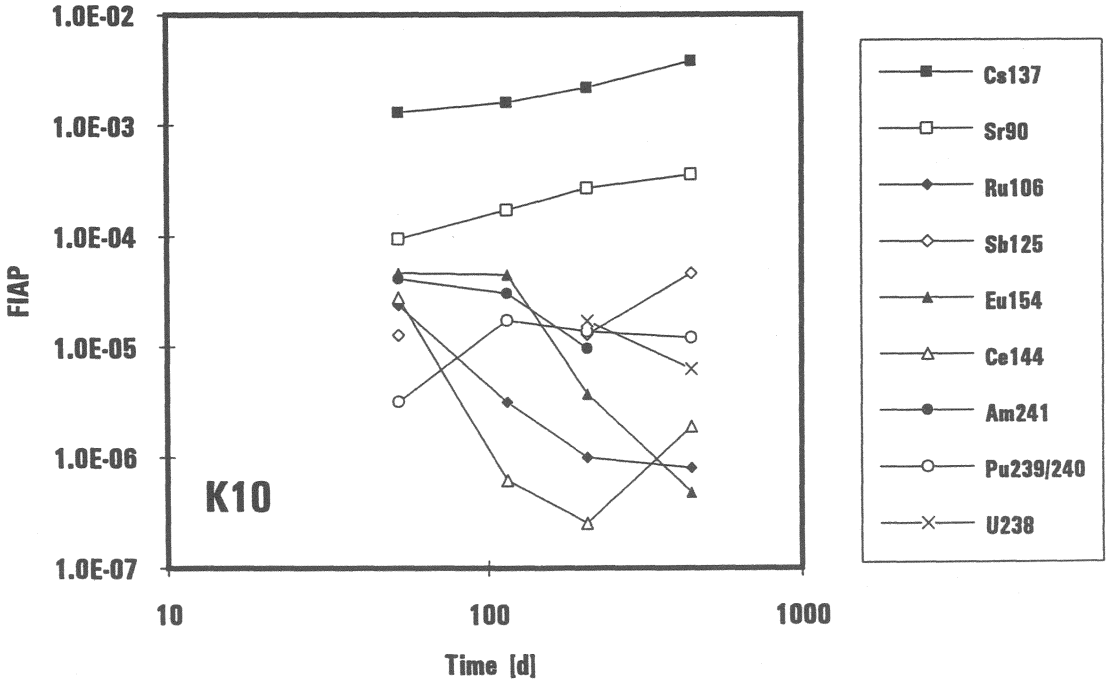

Fig.11. Spent fuel pellet (7.4 g) exposed to 200 mL 95% saturated NaCl solution. Fraction of inventories of various radionuclides in the aqueous phase (FIAP) Zircalloy cladding remained attached Note: Samples were washed twice in the leachant for periods of 1 month each. Data from wash solutions are not included in the Figures (see annual report 1992)

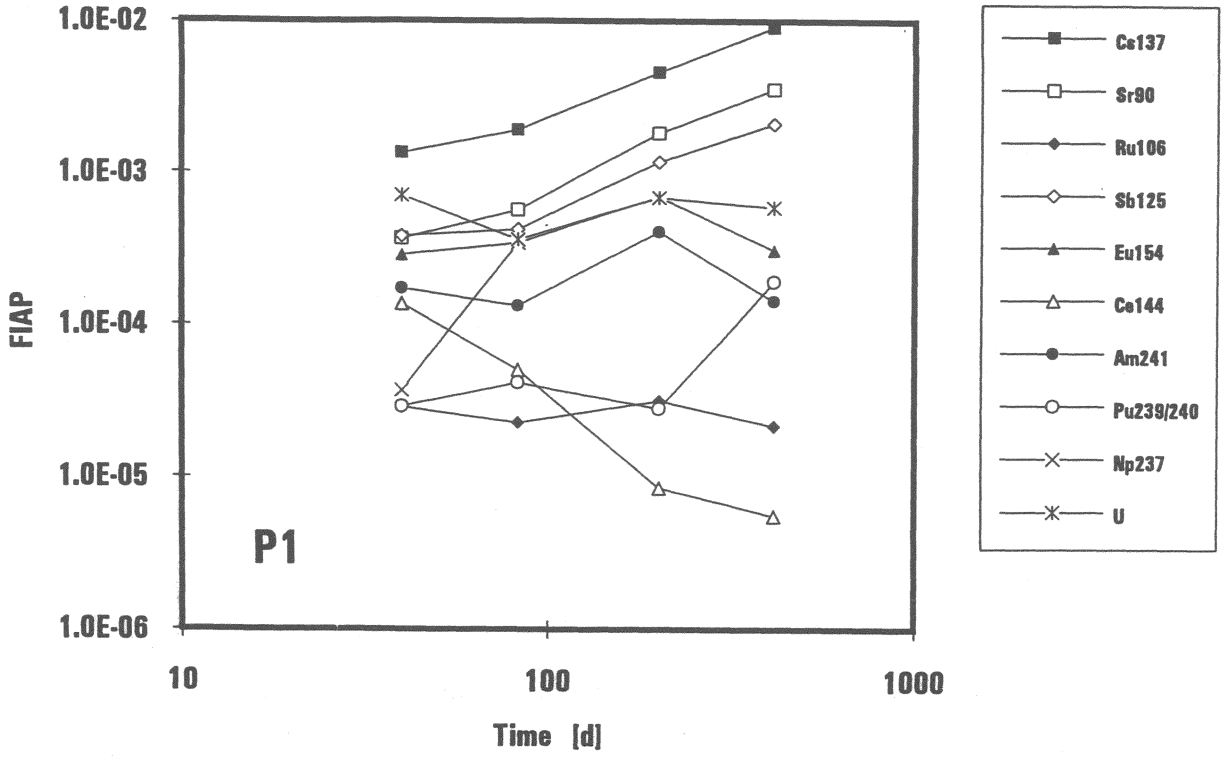

Fig.12. Spent fuel powder (2.9g, particle size < 3μm) exposed to 200 mL 95% saturated NaCl solution. Fraction of inventories of various radionuclides in the aqueous phase (FIAP). Zicralloy cladding was added to the test solution. Note: Samples were washed twice in the leachant for periods of 1 month each. Data from wash solutions are not included in the Figures (see annual report 1992)

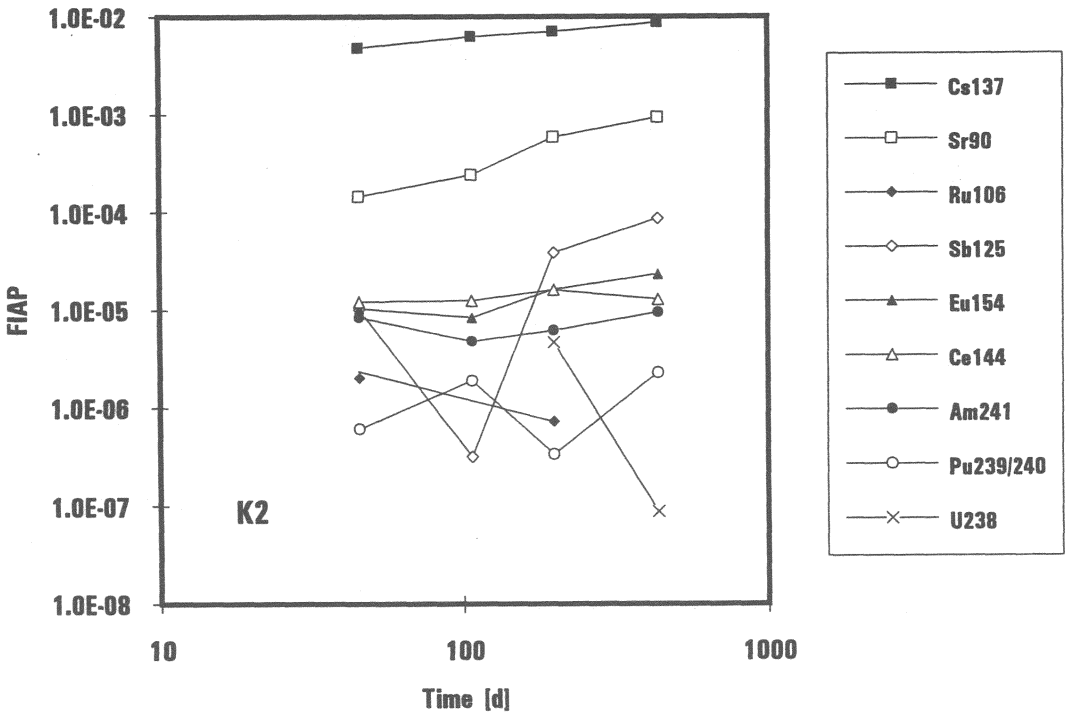

Fig.13. Spent fuel pellet (7.0 g) exposed to 200 mL deionized water. Fraction of inventories of various radionuclides in the aqueous phase (FIAP) Zircalloy cladding remained attached Note: Samples were washed twice in the leachant for periods of 1 month each. Data from wash solutions are not included in the Figures

Results from analyzing ultra filtered and micro filtered solution samples were the same for Ag, Sr, Sb, and Cs and differ slightly for actinides, Ru and rare earth elements but never by more than a factor of three. Colloid formation was not enhanced in the presence of fuel powder or of iron.

Fuel matrix behavior

Indicators for matrix behavior

Provided there is no segregation on fracture surfaces and grain boundaries, one may use the fastest dissolving nuclide as an indicator for fuel matrix dissolution and interprete lower values of other elements as controlled by secondary effects (i.e. sorption, (co-)precipitation). This procedure would gain plausibility if more than one element could be used as indicator for matrix degradation. Certain elements, like Cs, may only serve this purpose after the gap and accessible grain boundaries are washed out. After Cs134/137, in all tests Sr90 and thereafter Sb125 showed highest release values. Sr data are sometimes considered as measure for the degradation of the fuel matrix [Grambow et al. 1990a], due to homogeneous distribution in the fuel [Kleykamp 1985], but there are indications at least for high power fuel that Sr may become segregated in part (<5%) in perovskite phases [Jeffery 1967]. A discussion of Sr behavior during fuel dissolution is given in [Grambow et al. 1990b] Recent measurements for LWR fuel samples by Gray et al. [1992] indicated that not more than 0.1% of the total inventory of Sr90 was associated to grain boundaries, whereas measurements for CANDU fuel (high linear power) [Stroes-Gascoyne, 1993] indicate that the sum of gap and grain boundary inventories of Sr may become as high as 0.5 %. Our tests with fuel powders may provide additional insight because grain boundaries are exposed to the solution and grain boundary contents can be dissolved instantaneously. However, except during initial ultrasonic cleaning, initial Sr and U releases in the static tests are rather similar. This indicates that Sr is released from the matrix. With time the difference between the Sr and the U release data increases. This can be interpreted as resulting from a dissolution (Sr,U) / precipitation (U) mechanism. Hence, with time, data of Sr not of U are indicative of fuel matrix dissolution. Uranium may be bound to secondary precipitates (see below). From the difference in the initial fractions of inventories released from Sr and U during ultrasonic cleaning we may estimate an upper limit for the sum of gap and grain boundary inventories of Sr. This is not higher than 0.03 % of the total Sr inventory.

Maximum values for intrinsic fuel matrix dissolution rates

Using Sr90 as an indicator for matrix dissolution, matrix dissolution rates for the various experiments are given in Fig. 14 as a function of time. In general rates remain

constant with time. The decrease of release rates of Sr with time, as observed by Forsyth [1991], has not yet been observed in our experiments. Surface area normalized reaction rates may be estimated from these data using the surface area considerations discussed above under "experimental". Upper limits for intrinsic fuel dissolution rates ("forward reaction rates") may be obtained from tests with individual fuel fragments where saturation effects are negligible. We obtain a "forward" dissolution rate of about 5-7 mg/(m^2d) in 95% sat. NaCl solutions at 25°C. Our rate values are slightly higher than the value of about 2 mg/(m^2d) measured for spent fuel (ATM105, ATM106) in deionized water [Gray et al. 1991, 1993]. The differences may be attributed to the fact that the effective surface area is much higher than the geometric area used for our rate calculations. With this interpretation we would obtain a quite reasonable surface roughness factor of about 2.5 for our fuel. Considering an effective pellet surface area of 14 cm^2, Sr is released with a rather similar rate from fuel pellets of about 2 mg/(m^2d) in NaCl solutions and 6 mg/(m^2d) in deionized water .

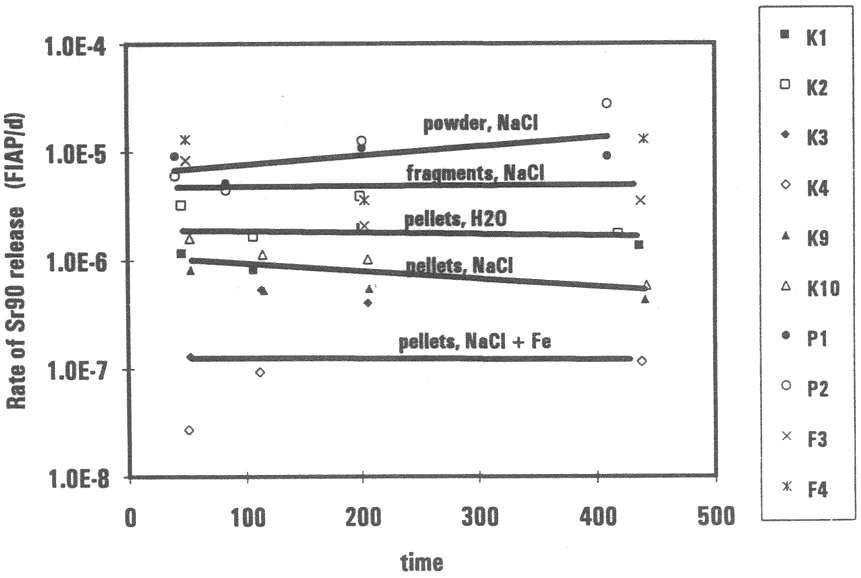

Fig. 14 . Influence of sample size and salinity on release rates of Sr90 from high burnup spent fuel at 25°C

Matrix dissolution rates lower than intrinsic rates: "Saturation effects" vs. radiolysis effects

Saturation effects may provide additional long-term stability for the fuel [6]. However, it is not clear whether these effects really occur under oxidizing conditions where UO_2 is unstabile. Our tests with powdered fuel may provide some more insight into this question. Table III contains NL_i and values for the dissolved fraction f_i of the contents of the various nuclides in a monolayer calculated from the measured radioactivities after the second sampling step after 83 days in a test with fuel powder. The corresponding upper limits for surface area normalized rates are 0.02-0.07 mg/(m^2d), much lower than intrinsic dissolution rates published in the literature [Gray et al. 1991, 1993] or estimated above from the present work. Corresponding depletion depths are in all cases, except for Cs (6 Å), lower than 2 Å.

Less than a monolayer of fuel was involved to account for the observed radionuclide releases. A monolayer of UO_2 may be considered to have a thickness of the minimum U-U distance of 3.87 Å in the crystal lattice (fluorite structure). The results show that for example only 4% of the Pu content of a monolayer is found in the aqueous phase. If only a monolayer is involved in the reaction it becomes meaningless to speak about a "matrix dissolution rate". Sorption and desorption phenomena and reactivities of individual crystallographic sites may dominate the behavior.

The pronounced decrease in the surface area normalized reaction rate with an increasing S/V ratio may be explained either by accumulation of dissolved reaction products in solution (saturation, solubility) or by enhanced depletion of reactants (dissolved oxygen, radiolytic products, i.e. H_2O_2, radicals, ClO^-, etc.) from solution. If, hypothetically, a fuel powder would be able to dissolve oxidatively with an intrinsic dissolution rate of 5 mg/(m^2d), it can be shown that this hypothetical process would consume radiogenic reactands faster than they are produced (generation rate of radiolysis products estimated from H_2 gas measurements). Hence, in the absence of other sources of oxidizing species, such high rates are impossible. In contrast, it could be that reaction rates in tests with powders are limited by the generation rate of oxidizing radiolysis products.

Table III Normalized mass losses NL_i [mg/m^2], and fraction fi of a monolayer after 83 days of static corrosion of 2.9 g of spent fuel powder in 200 mL 95% sat. NaCl solution at 25°C

	NL	f		NL	f
Ru106	0.06	0.015	Ag110m	0.03	0.007
Cs134	6.7	1.7	Am241	0.56	0.14
Cs137	6.3	1.7	Pu238	0.16	0.04
Sr90	2.0	0,51	Pu239	0.17	0.04
Eu154	0.44	0.11	U	1.06	0.27
Sb125	0.94	0.24	Np237	0.97	0.25
Ce144	0.14	0.04	Tc99	<0.9	<0.23

Effect of iron

The effect of iron and/or iron corrosion products on the mobility of radionuclides is illustrated by the data given in Fig. 15. The presence of iron effectively reduces the solution concentration of all radionuclides, except of Cs and fission gases (see above). The cumulative release of Cs was more than 4% of the inventory after 200 days, a value higher than the sum of gap and grain boundary inventories of fuel powder. The decrease in radionuclide mobility may indicate increased stability of the fuel matrix at the lower redox potential or may be due

to the fact that radiogenic oxygen is effectively consumed by iron corrosion. However, low release of other fission products and of actinides may alternatively be a result of sorption on iron. More work is necessary, before the effect of iron can be understood.

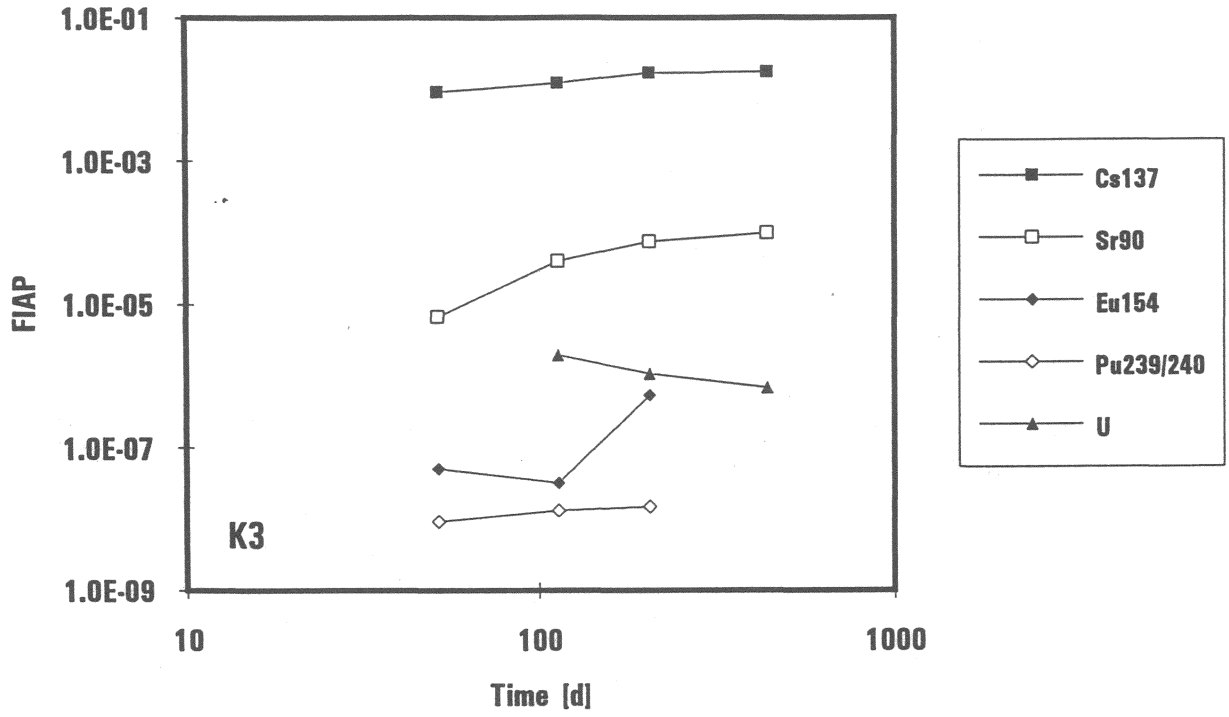

Fig.15: Effect of the presence of iron (8.5 g powder, grain size < 10 µm) on the dissolution process of a fuel pellet (7 g) in 200 mL 95% saturated NaCl solution. Fraction of inventories of various radionuclides in the aqueous phase (FIAP)

Behavior of radionuclides in the fuel dissolution process

Except for Cs, Sr and for Sb, the rating of radionuclides with respect to their FIAP values changes with the S/V ratio. The sequence is Cs>(Sr,Sb)>(Am, Eu)>(Ce,Pu,Ru) for powder (Fig. 12), whereas it is Cs>(Sr,Sb,Ru)>(Pu,Eu)>Ce with fragments (Fig. 10). The rating of the FIAP values is a function (1) of the relative significance of the individual contributions to radionuclide release from the fuel matrix, the fuel sheath gap, fracture surfaces and from grain boundaries, (2) of resorption processes onto the fuel surface or sorption on the Ta-container and (3) of (co-)precipitation processes. The above mentioned changes in the relative leachability of radionuclides may be rationalized in terms of reaction path considerations. The reaction path describes the change in solution composition and the formation of alteration phases as a function of reaction progress. In Fig..16 the solution

concentrations of various elements in the tests with NaCl solutions in the absence of iron at various S/V ratios are plotted against the reaction progress. Reaction progress is expressed in terms of the mass of fuel dissolved per unit mass of water. Sr-data are used to calculate the dissolved fuel mass, hence, solution concentrations of Sr must follow a straight line when plotted against reaction progress. Our experiments cover more than four orders of difference in reaction progress. Experiments with fuel fragments yield very low reaction progress values, highest reaction progress is obtained when using fuel powders. The concentration ranges observed in the various tests are summarized in Table IV.

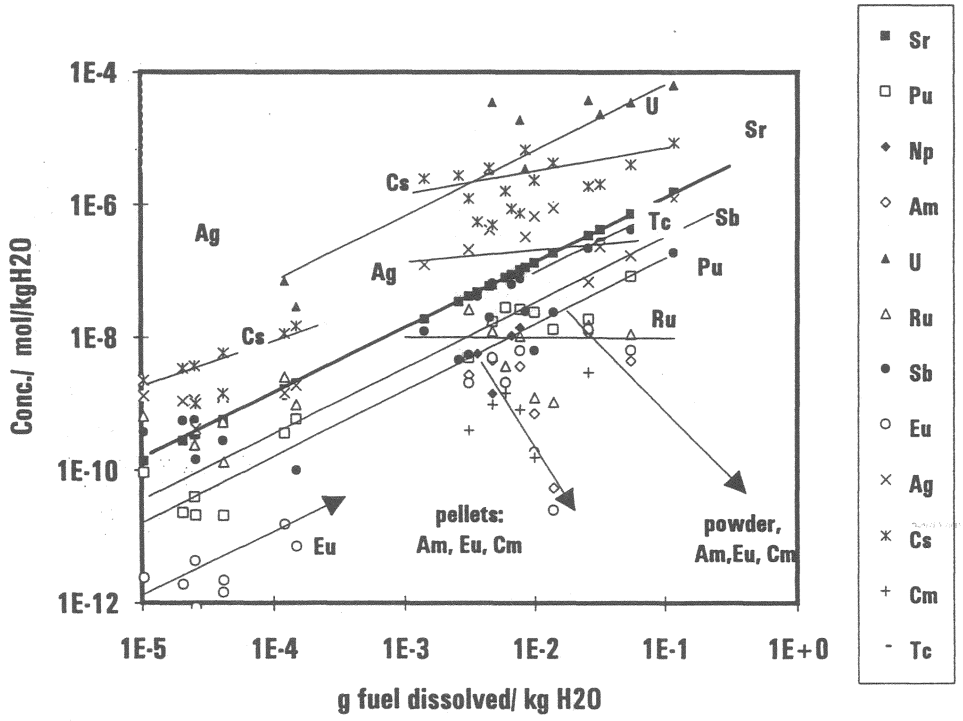

Fig.16: Solution concentrations of various elements in the tests with NaCl solutions (same data as in Fig. 10-12) plotted against the reaction progress. Reaction progress is expressed in terms of the mass of fuel dissolved per unit mass of water. Sr-data are used to calculate the dissolved fuel mass

Table IV: Range of concentrations (molal), observed in corrosion solutions, lower limits for Am, U, Np, Cm and Tc are detection limits

Sr	10^{-10}-10^{-6}	Cs	10^{-9}-10^{-5}
U	10^{-8}-10^{-4}	Pu	10^{-11}-10^{-7}
Eu	10^{-12}-10^{-8}	Am	10^{-9} -10^{-7}
Ru	10^{-10}-10^{-8}	Np	10^{-9} -10^{-8}
Sb	10^{-10}-10^{-7}	Cm	10^{-10}-10^{-9}
Tc	10^{-7}-10^{-7}	Ag	10^{-9} -10^{-6}

The solution concentrations of most elements increase with the proceeding reaction. Exceptions are Ru, whose concentration remains constant after reaching a concentration of

10^{-8} m (solubility?) and the elements Am, Cm and Eu with increasing concentrations a low reaction progress and decreasing concentrations at high reaction progress. Differences in the solution concentrations of the various elements are in part related to the different nuclide inventories in the fuel. Fig 17. gives the solution concentrations normalized to inventoryas a function of reaction progress. Normalized concentrations are expressed as g fuel/kg water. They may be interpreted as the hypothetical solution concentration of fuel if the fuel would dissolve with the same rate than the respective element. Data for Sr are again used for calculating reaction progress.

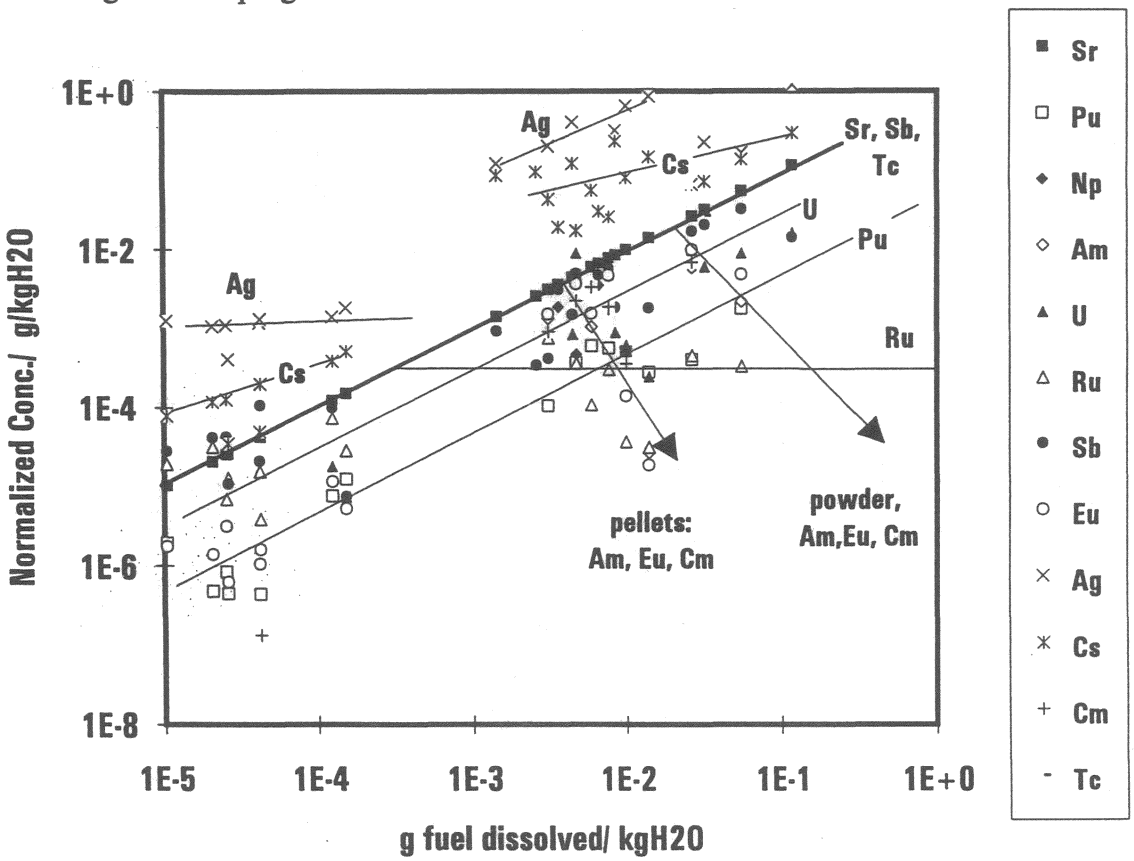

Fig.17: Normalized solution concentrations of various elements in the tests with NaCl solutions (same data as in Fig. 16)

Radionuclide release controlled by UO_2 matrix dissolution

Elements with normalized solution concentrations similar to those of Sr are released with the same rate, most likely as well being controlled by the dissolution of the fuel matrix. The kinetics of fuel matrix dissolution seem to control the release rates of Sr, Np, Tc, Sb and the initial release rate of Ru. It is surprising to find Ru being released by matrix dissolution as this element is contained in segregated metallic phases. Possibly, there is much more Ru in the fuel matrix than there is in segregated phases. It could also be possible that the metallic phases dissolve fast in chloride media.

Preferential release of radionuclides

When normalized solution concentrations of a given element are higher than the Sr data, preferential release from fractures, grain boundaries or easily soluble segregated phases is the likely cause. This is the case only for Cs and Ag.

Sorption and resorption controlling radionuclide release

Normalized concentrations of radionuclides lower than those of Sr are controlled either by sorption on the Ta-container or the zircalloy cladding, by resorption on the fuel samples, by precipitation or coprecipitation processes or by the dissolution of sparingly soluble seggregated phases. Among these elements are U, Pu, Am, Cm, Eu and Ru. If sorption, resorption, or sparingly soluble phases control release, the solution concentrations should increase with reaction progress, while they should decrease or remain constant in case of a controlling precipitation process. Coprecipitation may result in increasing, decreasing or constant concentrations with reaction progress, depending on endmember stability and stoichiometric constraints. At very low reaction progress (experiments with fuel fragments) normalized solution concentrations, except for Ru, are much lower than the Sr-data but solution concentration increase with reaction progress. It is likely that soprtion or resorption processes control release rates.

As an example one may discuss the the Pu data: Normalized Pu concentrations (as well as FIAP values, Fig. 17) are about a factor of 100 lower than the respective Sr data. Sorption may be described by equilibrium between the concentrations of Pu species in solution species and sorbed Pu species. In case of sorption or resorption being the only processes which remove Pu from solution, and in case solution concentrations of Sr are indicative for matrix dissolution an empirical mass distribution ratio R may be obtained:

$$R = Pu_{surface}/Pu_{solution} = NPu_{surface}/NPu_{solution}$$

where "Pu" and "NPu" denote masses and inventory normalized masses of Pu respectively. The mass balance may be written as

$$NPu_{surface}+NPu_{solution} = NPu_{dissolved} = NSr_{solution}$$

$NPu_{dissolved}$ is the normalized mass content of Pu in the dissoved fuel matrix. It follows that

$$NPu_{solution}/NSr_{solution} = 1/(1+R).$$

R depends on the solution chemistry of Pu, on the solution composition (incl. pH, Eh), on surface properties and on the ratio of surface area to solution volume (S/V). For a constant

chemical environment (fixed pH, Eh, pCO_2 etc.) and for conditions where sorption capacity and solublity limits are not exceeded R should be constant if the S/V is constant. With this rationale we may be able to distinguish sorption on the tantalum liner from resorption on the fuel sample solely by analyzing the effect of the S/V ratio on the mass distribution ratio. In case of sorption on the Ta liner its surface area S and S/V are constant, whereas for resorption on the fuel samples the surface area S and S/V vary by more than four orders of magnitude. As a distribution ratio of about 100 is observed for Pu, independent on the sample geometry and the associated sample surface area, it seems that sorption on the Ta liner is responsible for removing Pu from solution. Analysis of the Ta-container at the end of the tests will show whether this analysis is correct.

Behavior of potentially solubility limited nuclides

In order to rationalize solubility effects, the solution concentrations of radionuclides may be compared with the solubility of potentially precipitating phases.

Uranium

For U(VI) under oxidizing conditions a possibly solution concentrations controlling secondary phase is schoepite. Fig. 18. compares the measured solution concentrations of U as a function of pH with concentrations of U obtained from oversaturated conditions when titrating 5 m NaCl solutions with pure uranyl chloride solutions at a fixed pH value. The oversaturation experiments where performed for a period of three month, the dependence of uranium concentration with time is given in Fig.19, Schoepite was precipitating. There is good agreement between the uranium concentrations obtained in the dissolution test with fuel powders and the solution concentrations controlled by the precipitation of schoepite. Hence, it is possible that schoepite formation also controlls the uranium concentration in the powder test. Data at higher pH values (fuel pellets) may be compared with respective uranium concentrations obtained when dissolving of UO_2 in 5 m NaCl solution under an 21% O_2 atmosphere (see annual report 1992). There is good agreement, indicating that the same solid phase controlls uranium concentrations both in spent fuel tests and in tests with pure UO_2.

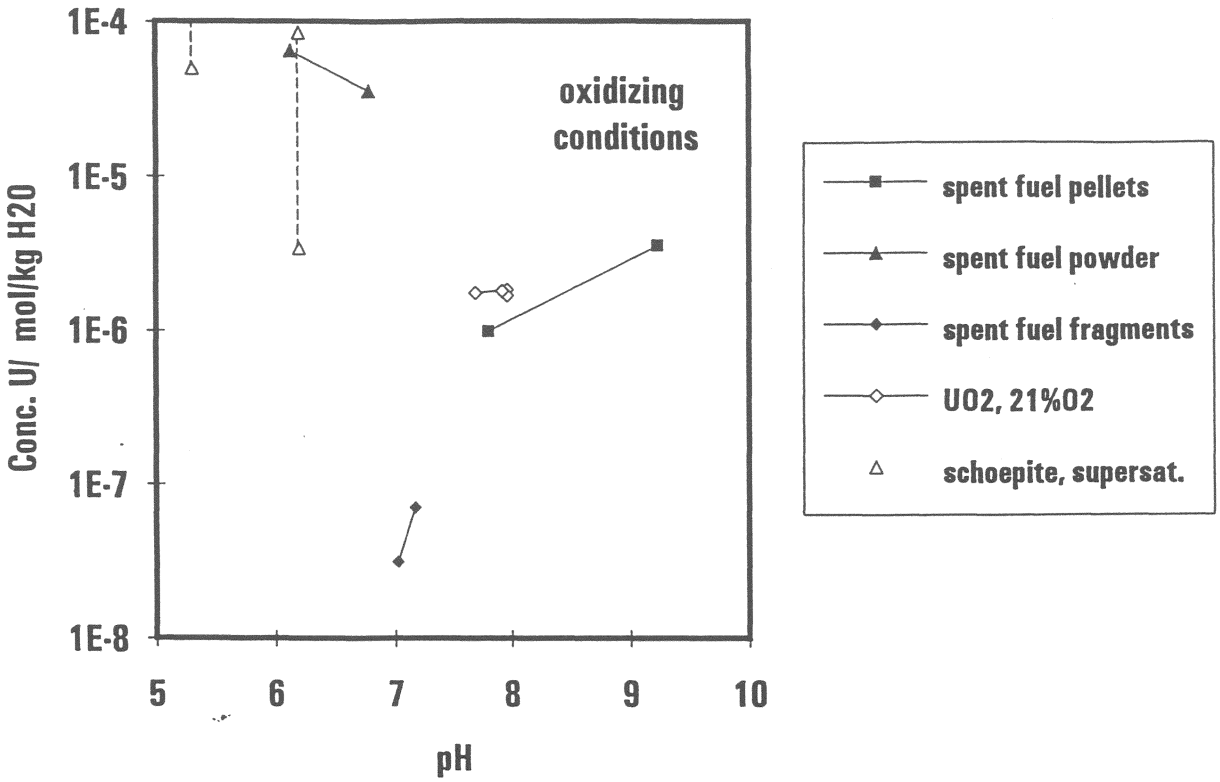

Fig 18. Uranium concentrations obtained in spent fuel dissolution tests in 95% saturated NaCl solutions at 25°C under argon atmosphere (contact time > 450d) Oxidizing reactands are produced by radiolysis

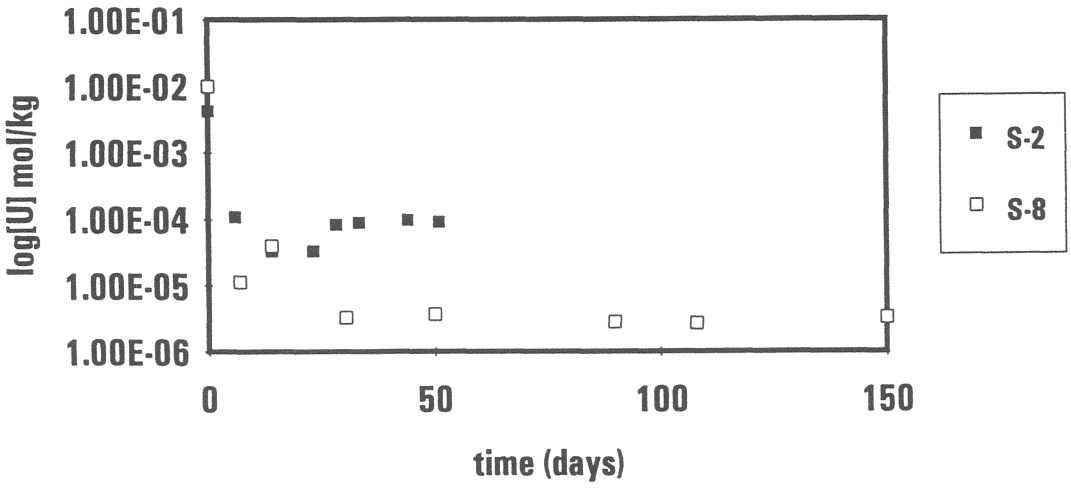

Fig. 19. Supersaturation test: Uranium concentrations after ultra filtration (1.8 nm) as a function of time. Titration of 5 m NaCl solutions with a UO2Cl2 at constant pH (6.3)). The formation of crystalline schoepite decreases the uranium concentration with time.Differences in the two data sets (S-2, S-8) are expected to result from differences in crystallinity.

The behavior of uranium under reducing conditions may be analyzed using the data from the test with iron powder being present. Fig. 20. shows that there is good aggreement between the measured solution concentrations of from the spent fuel tests and the uranium concentrations obtained when dissolving of UO_2 in 5 m NaCl solution under an H_2 atmosphere in presence

of Pd as a catalyst (see annual report 1992). This good aggreement suggests that reducing conditions are indeed achieved in the spent fuel experiments, hence, radiogenic oxidizing reactands are effectively removed from solution by reaction with the iron powder.

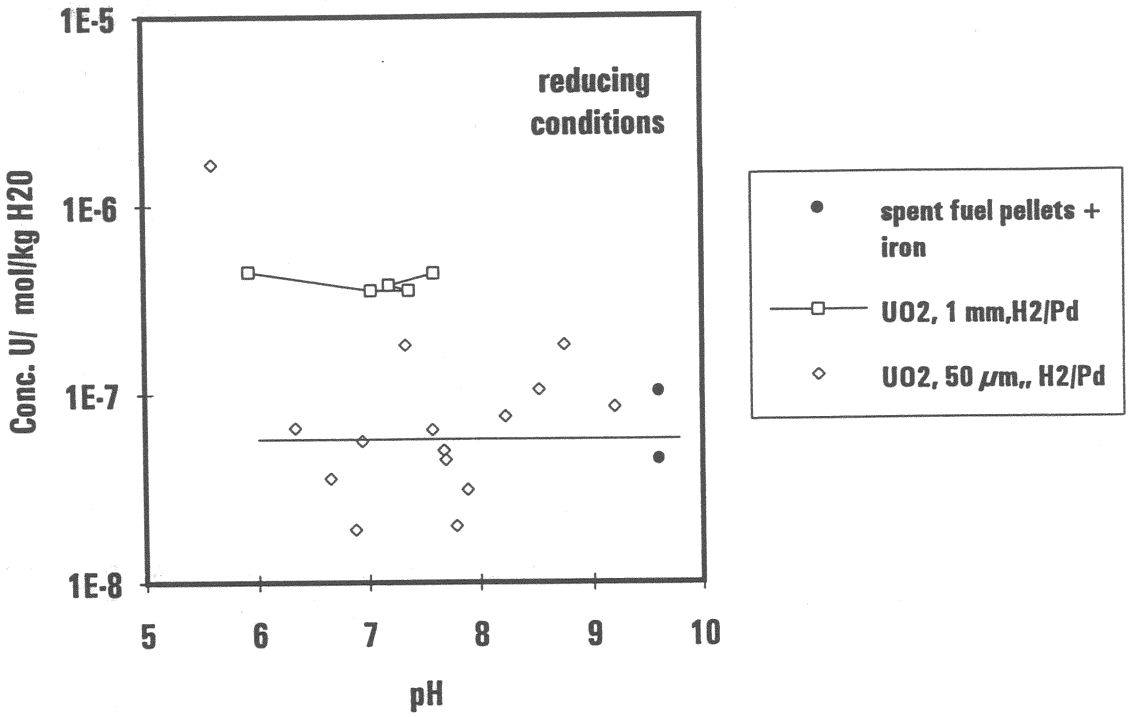

Fig. 20 Uranium concentrations in presence of Fe-powder, obtained in spent fuel dissolution tests in 95% saturated NaCl solutions at 25°C under argon atmosphere (contact time > 450d) Reducing conditions obtained by concumption of oxidizing reactands by reaction with Fe.

Americium, Curium, Europium

Measured Am concentrations are shown together with respective Eu concentrations in Fig.21. Eu and Am concentrations are always similar. Eu is easier detectable than Am, hence if Am is below the detection limit, we may use Eu data to deduce on the behavior of Am. Hypothetical maximum solution concentrations of Am were calculated (included in Fig. 21) with the assumption of congruent fuel matrix dissolution (using Sr as an indicator) by neglecting all secondary reactions which remove Am from solution (sorption, precipitation etc.). Measured solution are orders of magnitute below this maximum values, indicating that Am is effectively removed from solution. One of the processes which may reduce Am concentrations is the precipitation of secondary Am controlling phases. There exist few solubility measurements of Am in carbonate free anaerobic 5 m NaCl solutions [Stadler and Kim 1988, Runde 1993]. These data may serve as a point of reference for comparison. Adapting a model (based on the electrolyte theory of Pitzer and spectroscopic observations) for the ionic strength dependence of Cm hydrolysis to Am hydrolysis, Fanghänel et al. [1994] calculated the solubility of $Am(OH)_3$ in 5.8 m NaCl solutions and obtained good agreement with the data of Runde when using a solubility product at infinite dilution of log K = -28.2.

The calculated solubility data are included in Fig.21. Measured concentrations of Am/Eu in spent fuel corrosion solutions are about 5 orders of magnitude lower than the calculated values. One of the reasons for this discrepancy is the possible formation of solid solutions. The content of other trivalent cations in spent fuel (Nd, La, Pr, Sm..) is about 25 times higher than that of Am or Eu. It is rather unlikely that individuell Am(OH)3 phases will form. Instead, one expects the formation of solid solutions of the general type (REE;AN)(OH)3. Using the most simple solid solution model the partial solubility product $K_{p,SS}$ of a solid solution end member in a solid solution is

$$K_{p,SS} = f_i K_i$$

where f_i and K_i are the mol fraction of the endmember in the solid solution and the individual solubility product of the endmember in the absence of solid solution formation. Hence, if a solid solution forms with the stoichiometric ratios of Am and REE in the fuel, for Am(OH)3, $K_{p,SS}$ would be about 25 times smaller than $K_{i..}$ Solution concentrations calculated for this hypothesis are included in Fig.21 and cannot explain the observed behavior. More work is necessary to understand the behavior of trivalent rare earth and actinide elements.

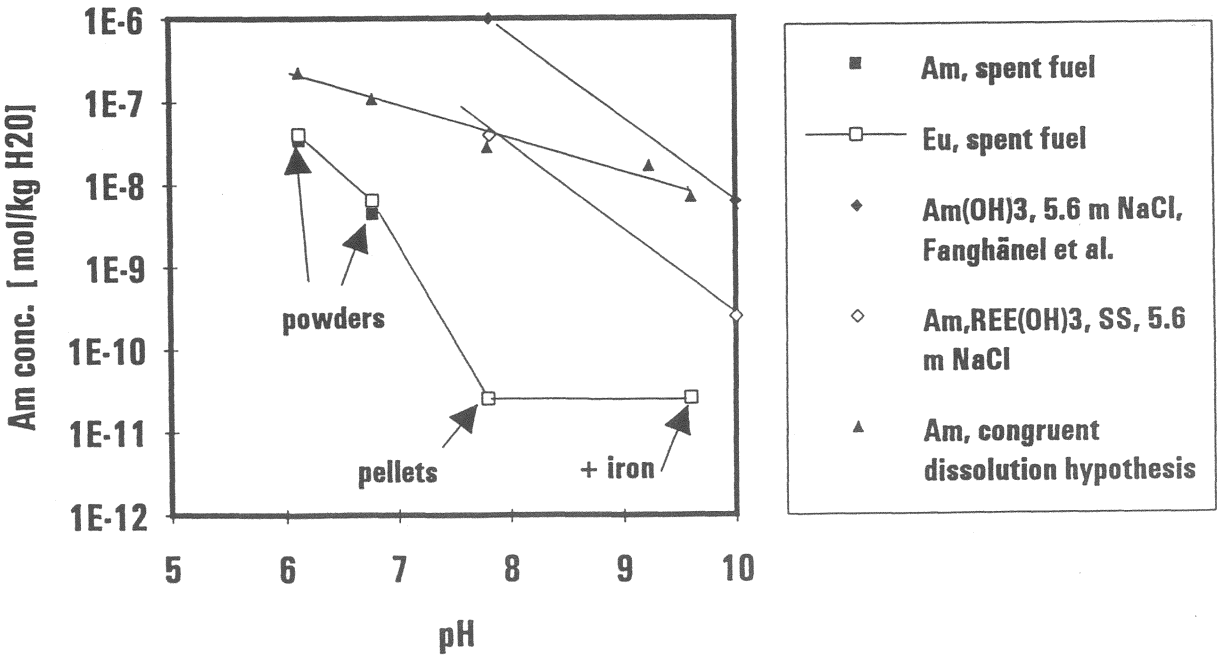

Fig..21 Am concentrations in spent fuel dissolution tests, compared with hypothetical solution concentrations of Am in the case that Am concentrations would be controlled by te rate of fuel matrix dissolution, or by the solubility of Am(OH)3 (Ref.) or by solid solution formation (see text)

Plutonium

Pu concentrations encountered in spent fuel dissolution tests in NaCl solutions are shown as a function of pH in Fig. 22 toghether with certain curves calculated for certain bounding cases. Pu-concentrations decrease with pH. Hypothetical maximum concentrations of Pu were calculated from the extend of matrix dissolution, using Sr data as reference and assuming that Pu is dissolved congruently without being involved in secondary reactions such as sorption, resorption, precipitation or coprecipitation.. Measured solution concentrations remain about a factor 100 lower than these values, clearly indicating that initially dissolved Pu is removed from solution by secondary reactions. As discussed above, sorption on the Ta-liner is a possible explanation of low Pu concentrations. Pu-concentrations, calculated for this process are included in Fig.., using a distribution constant R = 100. As can be seen there is fair agreement with the experimental data. Hence, the decrease of Pu-concentrations with increasing pH may be related to the decrease in the extend of fuel matrix dissolution with increasing pH. However, it cannot be ruled out that solubility processes control Pu concentrations in solution. Solubility calculations are complicated by the various possible oxidation states of Pu which may coexist simultaneously and by the possiblity that either Pu(IV) or Pu(VI) solid phases may form. In saline solutions at sufficiently high radiation doses, Pu(VI) is stabilized and lower oxidation states are oxidized by radiolysis [Pashalidis and Kim, 1988]. Pu(VI) solubility in carbonate free 5M NaCl solutions has been measured by Büppelmann and Kim [1988] and by Pashalidis and Kim [1992] at specific alpha activities between 148 and 1665 GBq/L and radiolytically induced Eh values >1000 mV. The solubility limiting phase in the experiments of Pasalidis and Kim [1992] was $PuO_2(OH)_2$. Reported experimental Pu concentrations were much higher than calculated solution concentrations based only on hydrolysis and chloride complexation. This increase was attributed to the formation of Pu(VI) hypochlorite complexes caused by alpha-radiolysis. For the pH range 6-10 of our experiments, the measurements by Pashalidis and Kim [1992] and by Büppelmann and Kim [1988] yield Pu concentrations which are always > $10^{-6.3}$ m, i.e. much higher than our Pu-concentrations. This difference may either be attributed to the lower alpha radiation doses and associated lower Eh values (in our test the specific alpha activity was always <10 GBq/L, Eh values were <0 mV), or Pu concentrations in our tests are not controlled by its individual solubility but by sorption, resorption (see discussion above) or by coprecipitation. Measurements of Pu(VI) solubility at low alpha doses are nor reported for 5 M NaCl solutions, we use for comparison to our data (included in Fig.. 22) the theoretical $PuO_2(OH)_2$ solubility curve calculated by Pashalidis and Kim [1992] by only considering hydrolysis and chloride complexation and neglecting radiolysis. It can be seen that measured solution concentrations remain lower than this solubility curve.

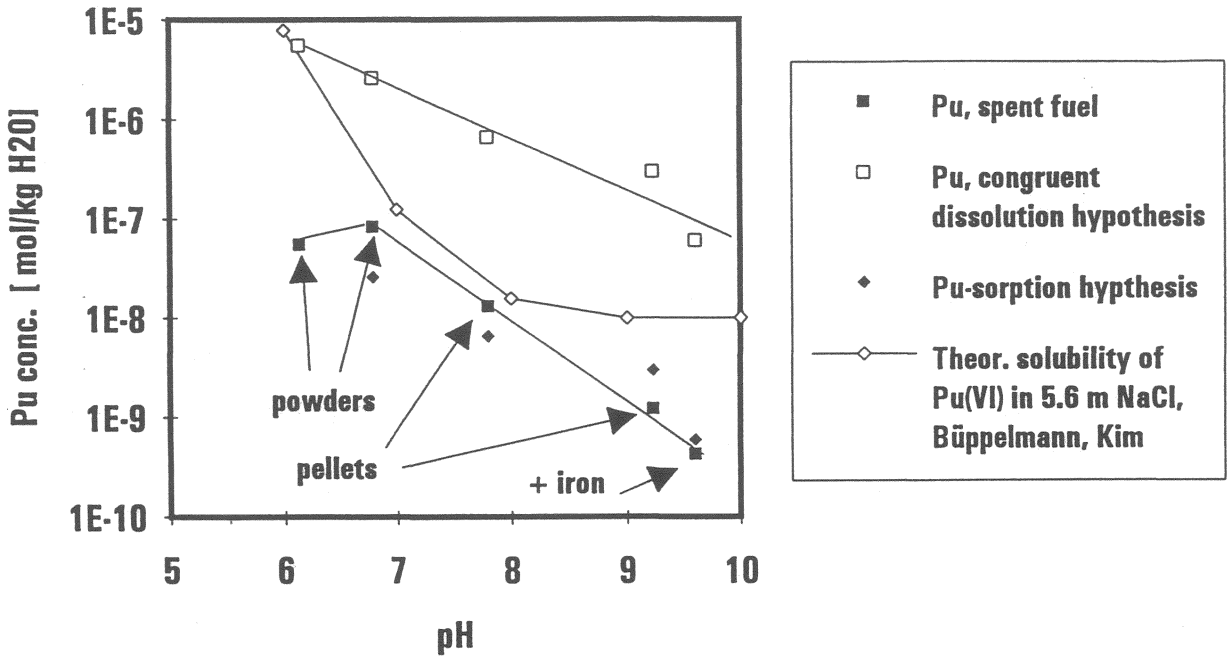

Fig. 22:.Pu concentrations observed in spent fuel dissolution tests in NaCl solutions as a function of pH. Comparison to theoretical solubility of PuO2(OH)2 [Büppelmann and Kim 1988], to sorption control of Pu and to Pu control by spent fuel matrix dissolution (see discussion in text)

1.3 CONCLUSIONS

Analyses of our results from spent fuel dissolution studies show that intrinsic dissolution rates cannot be used for long-term predictions in the case of only limited access of water to the fuel. If these rate would govern long-term fuel behavior a typically fractured spent fuel rod will become completely dissolved within 10^4 years after canister failure. Under anaerobic conditions with access of only small quantities of water, the fuel has a much higher stability, with reaction rates at least a factor of 100 lower than published intrinsic dissolution rates. This enhanced stability may be attributed to the consumption of radiolytic reactants.

1.4 ACKNOWLEDGEMENT

The authors are very thankful for the performance of hot cell work by **Mr. B. Schweigel** and **Mr. R. Reger** from the Department of Hot Cells (KfK) and of laboratory work by **Mr. Mr.N.Müller, Mr.W. Müller** and **Mr. R.Gebauer**. Help in the field of analytical work was gratefully obtained by **Mrs. A. Görtzen, Mr. K.Friese, Mr. F.Geyer** from INE (KfK).

1.5 REFERENCES

Büppelmann, K. und J.I.Kim, "Chemisches Verhalten von Plutonium in chloridhaltigen wäßrigen Lösungen"; Institut für Radiochemie der Technischen Universität München, RCM 01088 (1988)

Choppin, G.; Mater. Res. Soc. Symp. Proc. Vol. 176 (1990) pp. 449-456

Fischer, U.; H.W. Wiese, KfK 3014, Kernforschungszentrum Karlsruhe (1983)

Fanghänel, T, J.I. Kim, P. Paviet, R. Klenze, W. Hauser; Thermodynamics of radioactive trace elements in concentrated electrolyte solutions: Hydrolysis of Cm3+ in NaCl solutions" presented at the Migration 1993-Conference in Charleston, S.C., USA, and to be published in Radiochimica Acta (1994)

Forsyth, R.S.; Mat. Res. Soc. Symp. Proc. Vol. 212 (1991) pp. 177-188

Grambow, B., R.S. Forsyth, L.O. Werme, J. Bruno; Nuclear Technology 92 (2) (1990) pp. 204-13

Grambow, B.; L.O. Werme, R.S. Forsyth, J. Bruno, Mat. Res. Soc. Symp. Proc. Vol. 176 (1990) pp. 465-474

Gray, W.J. and D.M. Strachan, Mat. Res. Soc. Symp. Proc. Vol. 212 (1991) pp. 205-212

Gray, W.J., L.E. Thomas, R.E. Einzinger, Mat. Res. Soc. Symp. Proc. Vol. 294 (1993) pp. 47-54

Jeffery, B. M.; J. Nucl. Mater. 22 (1967) pp. 33-40

Johnson, L. and D.W. Shoesmith, in Radioactive Waste Forms for the Future, edited by W. Lutze and R.C. Ewing (North-Holland Publishers, Amsterdam, 1988) pp. 635-699

Kim, J.I.; Mat. Res. Soc. Symp. Proc. Vol. 294 (1993) pp. 3-21

Kleykamp, J. Nucl. Mater., 131 (1985) p. 221

Pashalidis, I., and J.I.Kim, "Chemisches Verhalten von sechswertigem Plutonium in konzentrierten NaCl Lösungen unter dem Einfluß der eigenen alpha-Strahlung"; Institut für Radiochemie der Technischen Universität München, RCM 01092 (1992)

Runde, W.; "Zum chemischen Verhalten von drei- und fünfwertigem Americium in salinen NaCl-Lösungen" Dissertation, Technische Universität München, (1993)

Stadler, S. und J.I.Kim, "Chemisches Verhalten von Americium in natürlichen wäßrigen Lösungen: Hydrolyse, Radiolyse und Redox-Reaktionen"; Institut für Radiochemie der Technischen Universität München, RCM 01188 (1988)

Stumm, W. and J.J.Morgan, "Aquatic Chemistry"; John Wiley & Sons, New York (1981)

Stroes-Gascoyne, S. et al.; Mat. Res. Soc. Symp. Proc. Vol. 294 (1993) pp. 41-46

2. CORROSION TESTS WITH UNIRRADIATED UO_2 (s)

2.1 INFLUENCE OF THE PARTICLE SIZE

In the last annual report, we discussed a mathematical oxidation-dissolution model of UO_2 under oxidizing conditions, which described a mechanism based on the oxidation of the UO_2 surface and a fast dissolution of this oxidized layer. This mechanism implies that the UO_2 surface would have a composition near to $UO_{2.1}$. However, surface analysis carried out by using X-Ray Photoelectronic Spectroscopy (XPS) have shown a higher oxidized layer close to $UO_{2.33}$ [1].

In this report, the dissolution of UO_2 has been studied as a function of pH and initial sample treatment under oxidizing conditions. During the dissolution experiment, several solid samples were removed from the vessel at different time and analyzed by XPS in order to determine the U(VI)/U(IV) ratio on the surface.

2.1.1 EXPERIMENTAL

Unirradiated UO_2 pellets were crashed and sieved, and two different particle size ranges were used in this work: 100-300 and 900-1100 microns. Surface area determined by the BET method gave 0.0113 $m^2\ g^{-1}$ and 0.0016 $m^2\ g^{-1}$, respectively.

The solid (7.8 g) was put in contact with 150 ml of 0.01 mol L^{-1} $NaClO_4$ in two different Teflon vessels. The pH was adjusted in each vessel to 4 or 8 by adding $HClO_4$ or CO_2-free NaOH solutions, respectively. The pH was measured by means of a combined glass electrode. Oxidizing conditions were achieved by using 5% O_2 in N_2 flux. The redox potential was continuously recorded by means of a platinum wire, using a Ag/AgCl reference electrode. The experiments were carried out at room temperature.

The uranium concentration in aqueous phase was determined as a function of time using a sequential methodology. All samples were immediately filtered through a 0.22 microns MILLIPORE membrane filter, and uranium concentration was determined by the Scintrex UA-3 uranium analyzer [2].

In order to understand the overall dissolution process, the evolution of the solid surface during the experiments has been studied. Solid samples of the experiments carried out at pH=4 and 8 were removed at different times. Samples were dried at vacuum during 24 hours and the U(VI)/U(IV) ratio on the solid surface was determined by using X-Ray

Photoelectron Spectroscopy with a PHI-Perkin Elmer ESCA System Multianalyzer 5500. The resolution of the $U_{4f7/2}$ peak of the XPS spectrum allowed the determination of the percentage of U(IV) and U(VI) on the surface [3].

2.1.2 RESULTS

The moles of uranium released as a function of time at pH= 4 and 8 are plotted in figure 2.1.1. A decrease of the release rate is observed in both cases after a relatively fast initial dissolution. This general behavior has been shown in dissolution studies of both spent fuel and unirradiated UO_2 [4,5]. Recently, a slow increase of uranium concentration has been reported to occur even after 5 years of leaching experiments [6] in absence of carbonate. The initial release has been explained taking into account an oxidized surface layer which dissolves very easily [7]. This fact has also been observed in experiments carried out at reducing conditions [8].

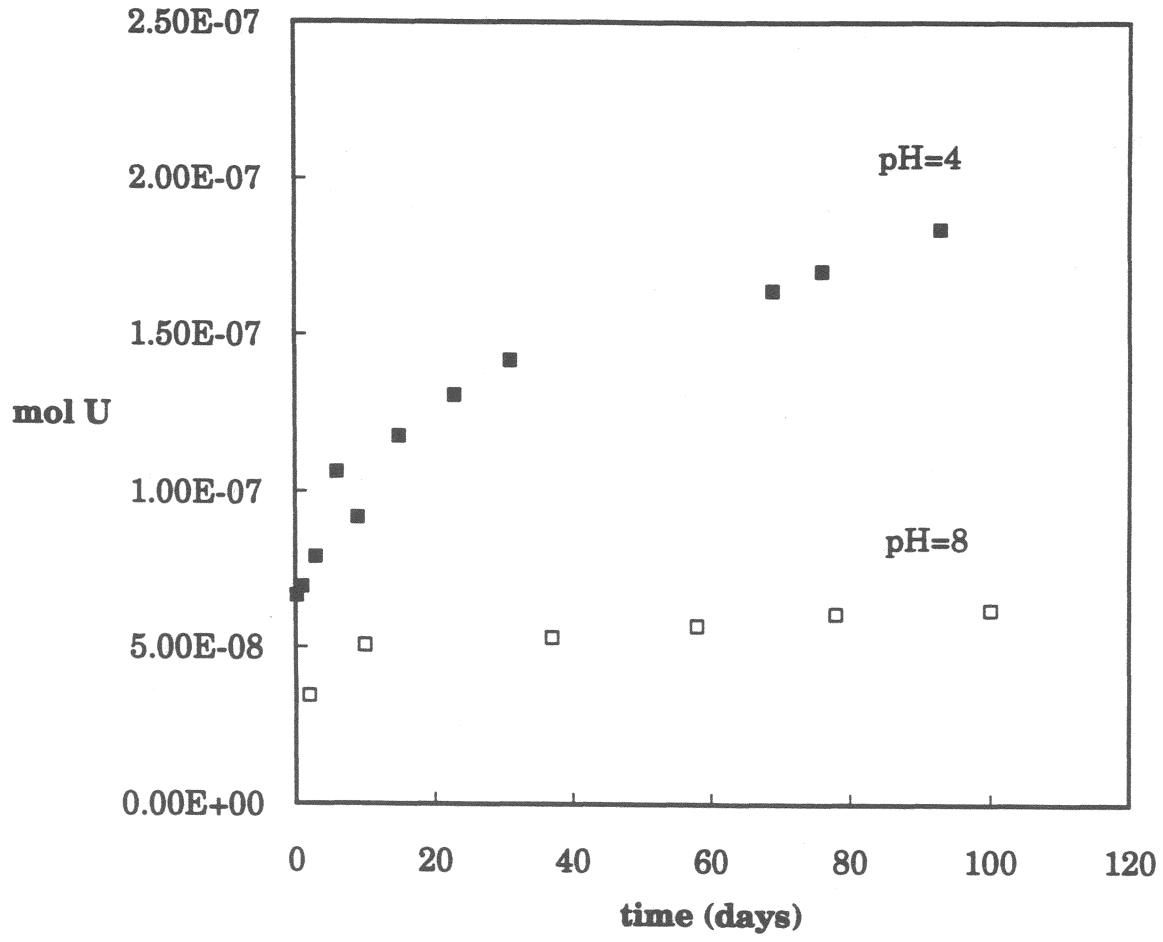

Fig. 2.1.1: Uranium release as a function of time at two different pH values.

In order to confirm the presence of an oxidized surface layer, two experiments were carried out at the same conditions. In one case, the solid sample was washed with diluted perchloric acid and degassed distilled water several times before starting the experiment. In the other case the solid was not pretreated. Results are shown in figure 2.1.2. As it can be seen, the uranium release during the first days is found to be higher when the solid is not pretreated. This fact demonstrates the presence of an initial oxidized surface which is not completely removed by the treatment used in this work, since the change of the slope can still be seen in the experiment.

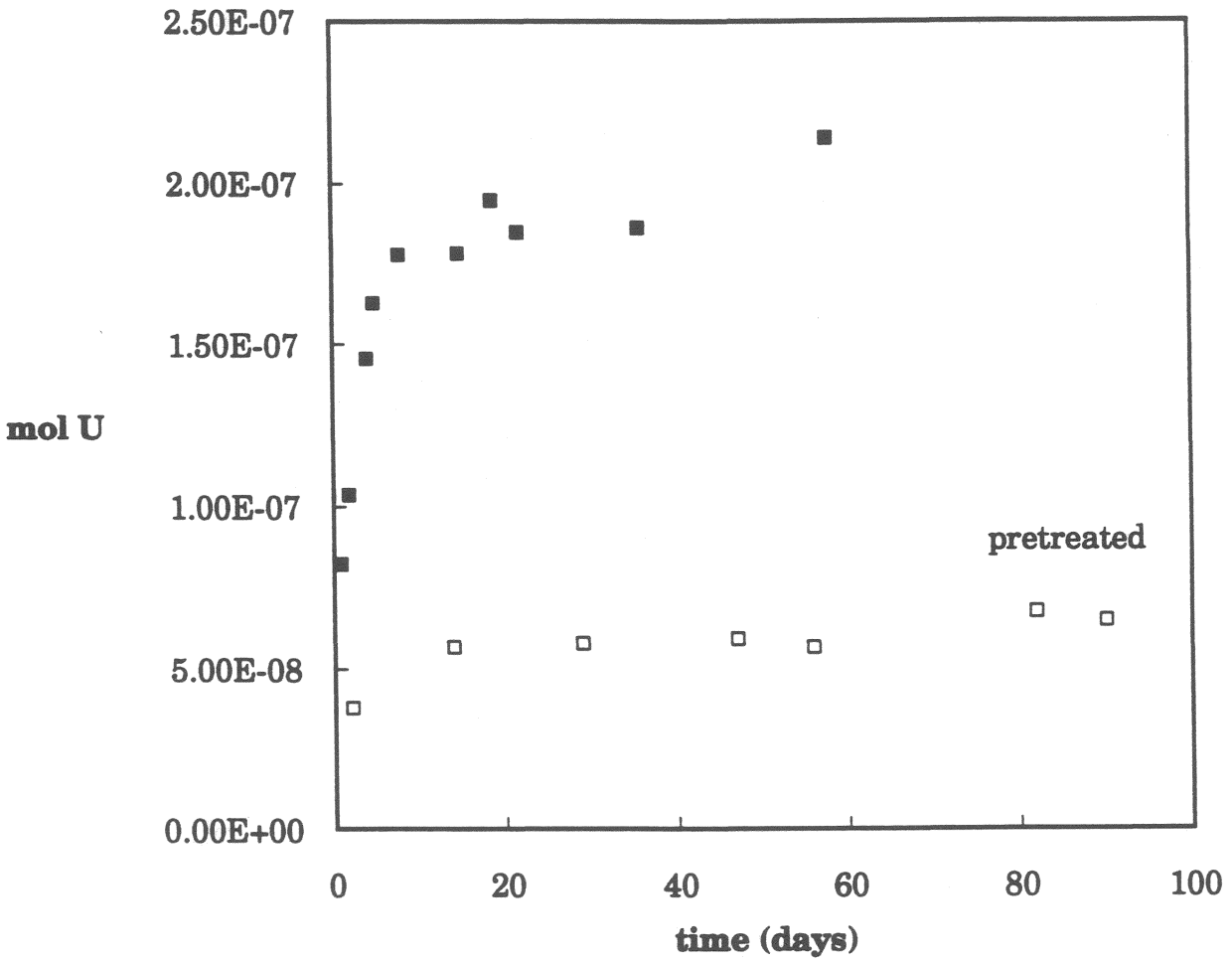

Fig. 2.1.2: Uranium release as a function of time at pH 8 and different initial treatment.

The solid surface characterizations are resumed in Table 2.1.1. These values show that the initial solid surface is rather oxidized, and decreases during the first days of leaching increasing again at basic pH up to values close to U_3O_7. On the other hand, at acid pH the solid surface is less oxidized at the end of the experiment with a value near to $UO_{2.1}$. Similar observations have also been reported by Shoesmith et al [1]

Table 2.1.1. XPS determinations of UO_2 surface as a function of time.

pH	Time (days)	% U(VI)	% U(IV)
8	0	60	40
8	2	12	88
8	4	23	77
8	37	38	62
8	102	39	61
4	0	71	29
4	20	27	73
4	100	10	90

2.1.3 DISCUSSION

From the XPS results, it is clear that the manipulation of the unirradiated UO_2 in air leads to the formation of an oxidized layer on the solid surface. The initial dissolution would correspond to the dissolution of this layer. The dissolution of this initial oxidized layer is found to be relatively fast, since the percentage of U(VI) on the solid surface clearly decreases in two days under the experimental conditions (see Table 2.1.1).

As a subsequent step on the dissolution mechanism, the UO_2 is oxidized by the oxygen dissolved. At pH = 8, the composition of the solid surface after the experimental time is close to U_3O_7, which corresponds to a O/U ratio higher than the one found at pH = 4 for the same experimental time.

Based on the experimental observations, we present the hypothetical mechanism of dissolution schematically depicted in figure 2.1.3.

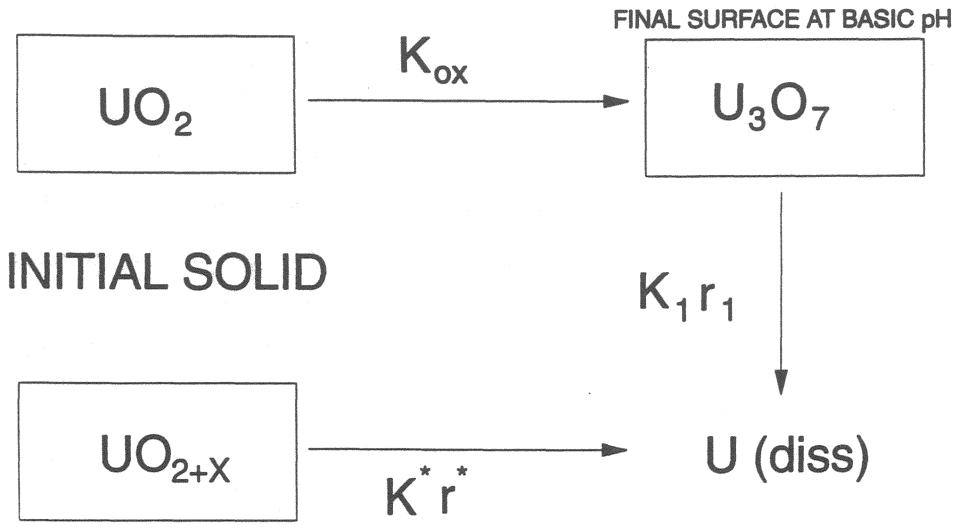

Fig. 2.1. 3 : Scheme of the hypothetical mechanism of UO2 dissolution under oxidizing conditions.

As it has been shown, the evolution of the solid surface is very important to understand the overall mechanism. Therefore, a mathematical model has been developed assuming a surface evolution during the experiment as it shown in table 2.1.2.

The moles of uranium released as a function of time will depend on the dissolution of UO_{2+x} and U_3O_7, following the expression:

$$dmU / dt = S_1 r_1 + S^* r^*$$

where **mU** is the total uranium dissolved, **t** is the elapsed time and $\mathbf{r_1}$ and **r*** are the U_3O_7 and the UO_{2+x} dissolution rates respectively.

Table 2.1.2: Composition of the solid surface

Solid	Surface	Initial Surface
UO_{2+x}	S^*	$S_{0^*} = w^* S$
UO_2	S_0	$S_{00} = w_0 S$
U_3O_7	S_1	$S_{10} = w_1 S$

As we discussed in the last annual report, UO_2 dissolution has been neglected because its solubility limit is lower than the uranium concentration measured and the approach of a pseudo-zeroth order kinetic has been made taking into account that the uranium concentration is far from the equilibrium concentration of an oxidized phase such as schoepite at the conditions of this work. Therefore, $\mathbf{r_1}$ and $\mathbf{r^*}$ values will be constant with time and the uranium released will depend on surface variation as it has been shown in the XPS determinations.

During the dissolution, the total surface remains constant but the surface of the different oxides change. In the case of UO_2 surface (S_0), we have:

$$dS_o / dt = - K_{ox}S_o + K^*r^*S^* + K_1r_1S_1$$

where the first term refers to the oxidation, the second to the UO_{2+x} dissolution and the last one to the U_3O_7 dissolution. K^* and K_1 values take into account the increase of S_o area with the dissolution of UO_{2+x} and U_3O_7, because we suppose that there is UO_2 under the oxidized layer. We have supposed that these two values are constant with time because we have assumed that the increase of S_o is proportional to moles released of UO_{2+x} and U_3O_7.. K_{ox} is the effective number of oxidations per time unit.

On the other hand, UO_{2+x} disappears following the expression:

$$dS^* / dt = -K^*r^*S^*$$

solving this equation, we obtain:

$$S^* = S^*_0 e^{-K^*r^*t}$$

This expression shows that S^* decreases from an initial value to dissappear after some time given by $K^*.r^*$.

As it was mentioned above, the total surface is constant and it is the sum of each surface:

$$S=S_1+S_0+S^*$$

thus:

$$dS_o / dt = SK_1r_1 - S_oK' + S_o*(K*r* - K_1r_1)\ e^{-K*r*t}$$

where $K'=K_{ox}+K_1r_1$.

This differential equation can be solved if we choose a particular solution with a constant and one exponential term. We have taken as boundary condition the value S_{00} for t=0. An expresion of S_0 as a function of time is obtained:

$$S_o = S[w_oe_1 + (K_1r_1 / K')\ (1 - e_1) + w*p(e_1 - e_2)]$$

where:

$$e_1=e^{-K\not{t}t}$$

$$p = (K*r* - K_1r_1) / (K*r* - K')$$

$$e_2=e^{-K^*r^*t}$$

These expresions show that the initial oxidized layer dissapears with time, giving the final solid surface. In figure 2.1.4, the surface variation is plotted as a function of time. The final solid surface is given by:

$$S_{1_{final}}=S(K_{ox}/K_{ox}+K_1r_1)$$

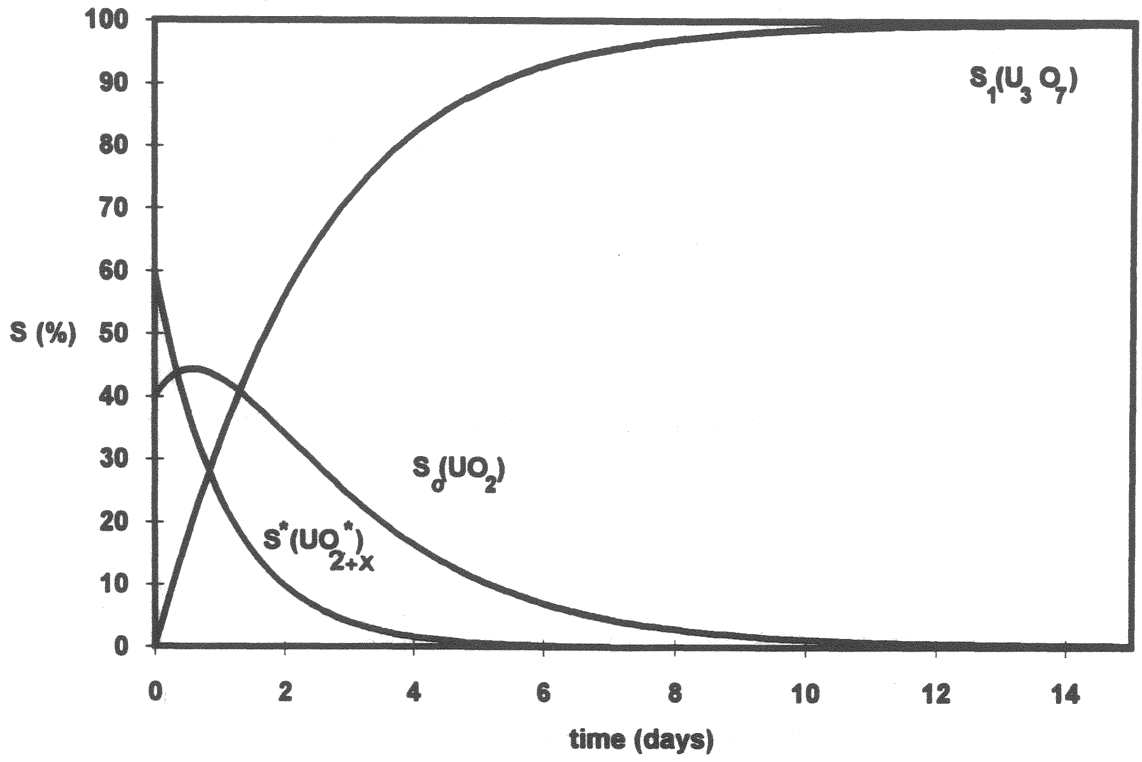

Fig. 2.1.4: Surface variation predicted by the model at basic pH as a function of time.

These final expressions can explain the effect of pH observed in this work. At basic pH, K_{ox} is higher than K_1r_1, thus the final surface is close to U_3O_7. Whereas, at acid pH, K_1r_1 is higher than K_{ox}, and the final surface is close to UO_2. This fact agrees with the results of different authors which point out that the dissolution rate is higher at acid pH.

Once, the expressions of the variation of the surfaces have been obtained, the integration of the general uranium moles released can be made. The following expression is obtained with mU=0 for t=0:

$$mU = r_1 S \left[\frac{K_{ox}}{K'} t + \frac{1}{K'} \left[w_1 + (1+p)\, w^* - \frac{K_{ox}}{K'} \right] (1-e_1) + \frac{w^*}{K^* r^*} (1-e_2) \left(\frac{r^*}{r_1} - 1 - p \right) \right]$$

This general model has been applied to the dissolution experiment carried out in paralel with XPS determinations of the solid surface. In this experiment, taking into account the general mechanism proposed, two different rates can be written:

$$\left(\frac{dmU}{dt} \right)_{final} = r_1 S \frac{K_{ox}}{K'} = m$$

In the final zone, the uranium moles realesed increase linearly with time, thus:

$$\left(\frac{dmU}{dt}\right)_{initial} = r^* Sw^* + r_1 Sw_1$$

$$mU = mt + b$$

where **b** is:

$$b = r_1 S\left[\frac{1}{K'}\left[w_1 + (1+p)\,w^* - \frac{K_{ox}}{K'}\right] + \frac{w^*}{K^* r^*}\left(\frac{r^*}{r_1} - 1 - p\right)\right]$$

This term corresponds to the uranium moles dissolved during the first part of the experiment, when the solid surface is not constant. For this experiment, we obtained: m = 8.1 10^{-10} mol/day and b = 1.6 10^{-7} mol

Figure 2.1.5 shows the experimental dissolution values fitted by the mathematical model as well as the composition of the solid surface at different time.

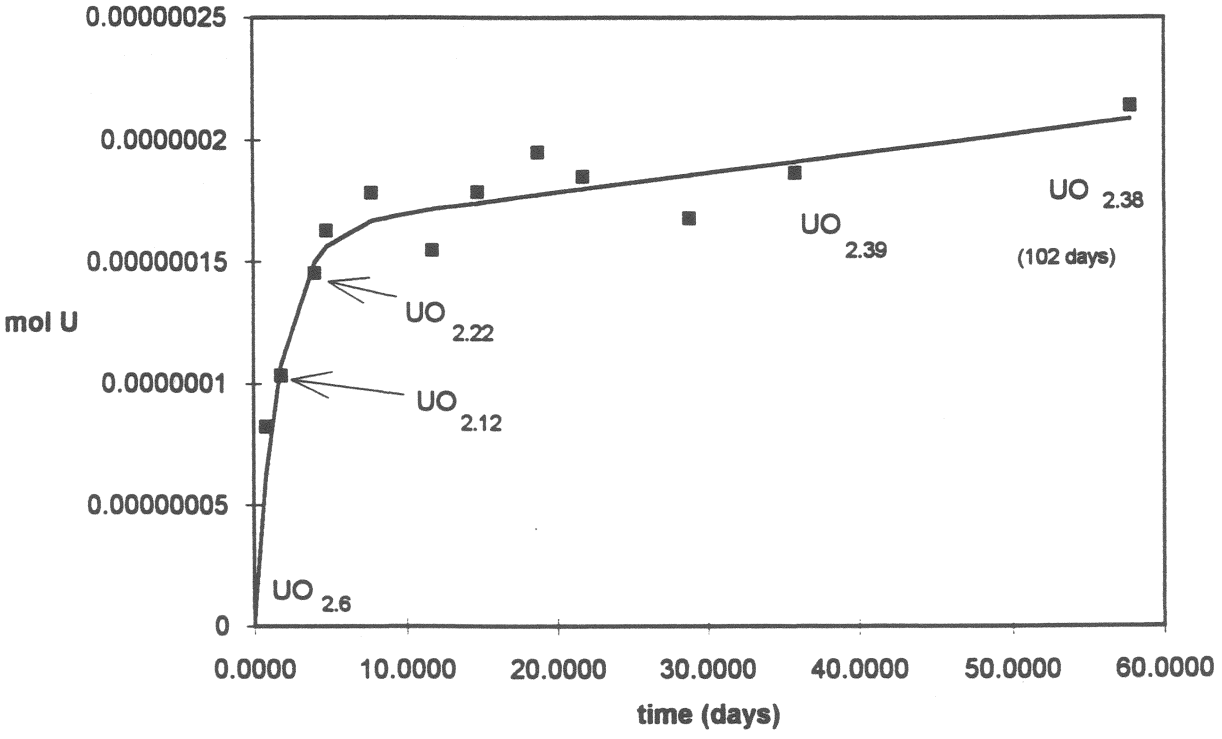

Fig. 2.1.5: Experimental data fitted by the model. Evolution of the solid surface composition during the experiment.

The parameters calculated by fitting the mathematical model to the dissolution data have been used to predict the composition of the solid surface as a function of time. This composition is compared to the XPS results in figure 2.1.6. Good agreement can be observed.

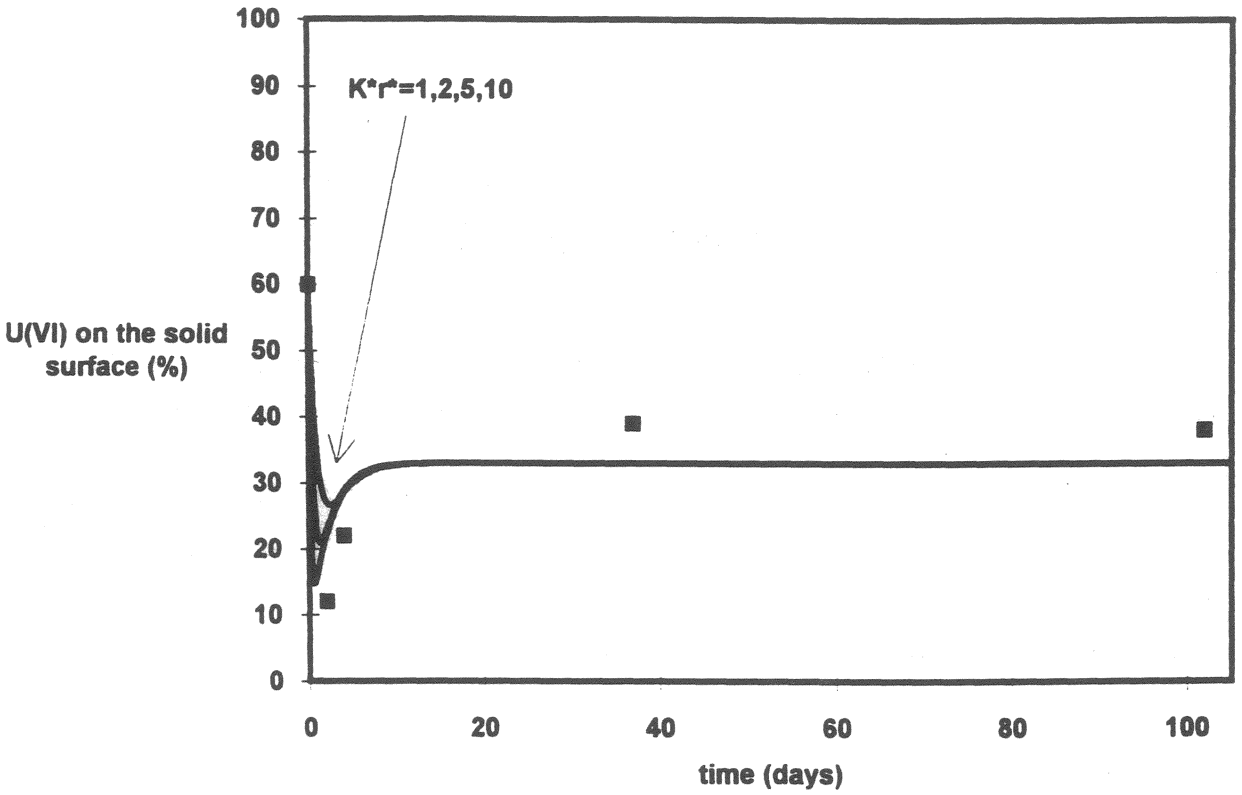

Fig. 2.1.6: XPS surface oxidation percentage versus time fitted by the kinetic parameters.

However, some aspects have to be studied in more detail i.e. the low dissolution rate attributed to the U_3O_7. In our model, we have assumed no precipitation of secondary phases. This point is not clear, since U(VI)-H_2O system is not completely understood. In this context, the U_3O_7 dissolution rate (K_1r_1) in the model could be due to more than one elementary reaction. Further studies should be done to clarify this supposition.

2.2 DISSOLUTION OF UO_2 (s) IN BRINES

In the last annual report, we presented results on UO_2 dissolution in Q-brine as a function of oxigen partial pressure. In the same context, we have studied this year the UO_2 dissolution in NaCl-brine under different redox conditions such as: reducing in hydrogen; anoxic with nitrogen and oxidizing in air CO_2-free.

2.2.1 EXPERIMENTAL

The solid phase used was an unirradiated crystalline UO_2 with 1 mm particle size. The same size used in Q-brine experiments. The specific surface area of the solid is 0.0016 m^2/g, determined by the BET methodology.

NaCl brine was prepared by dissolving 176.4 g of NaCl, 2.2 g of $MgSO_4$ 7H2O, 1.8 g of $CaSO_4$ $2H_2O$ and 1.6 of K_2SO_4 in 500 g of water [9]. The pH is 7.5.

Reducing conditions were achieved by bubbling hydrogen into the experimental vessel using a Pd catalyst, anoxic conditions were maintened with nitrogen and an air flux was used to obtain oxidizing conditions.

Uranium concentration was determined by the SCINTREX laser fluorescence technique [2] after a sample work-up previously developed [10].

2.2.2 RESULTS AND DISCUSSION

The results obtained in terms of total uranium concentration in NaCl-brine as a function of contact time are plotted in figures 2.2.1, 2.2.2 and 2.2.3.

The UO_2 dissolution under reducing condition (fig 2.2.1) follows the general behaviour at these conditions. An initial release of uranium during the first days of the experiment followed by a decrease of the concentration attributed to the precipitation of a uranium (IV) hydroxide. The final value obtained agrees with the solubility of UO_2 determined at 5 m NaCl at the same conditions.

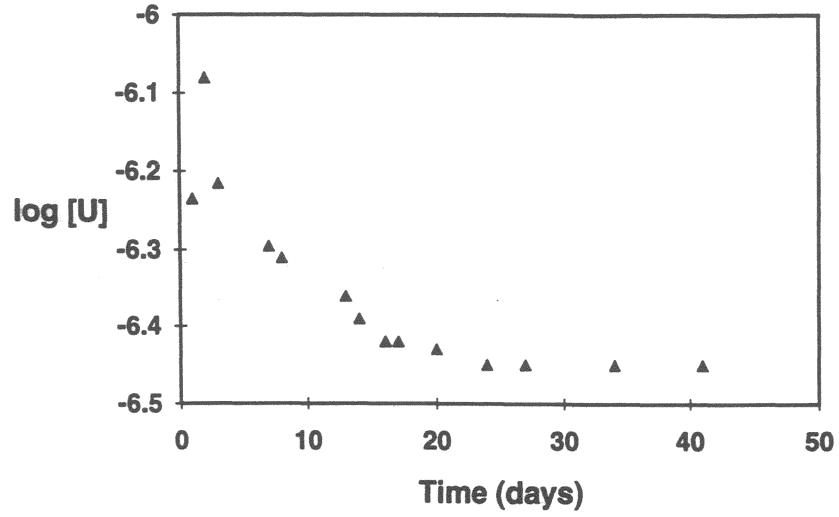

Fig. 2.2.1: Uranium concentration versus time under reducing conditions (NaCl-brine in 100% hydrogen with Pd catalyst).

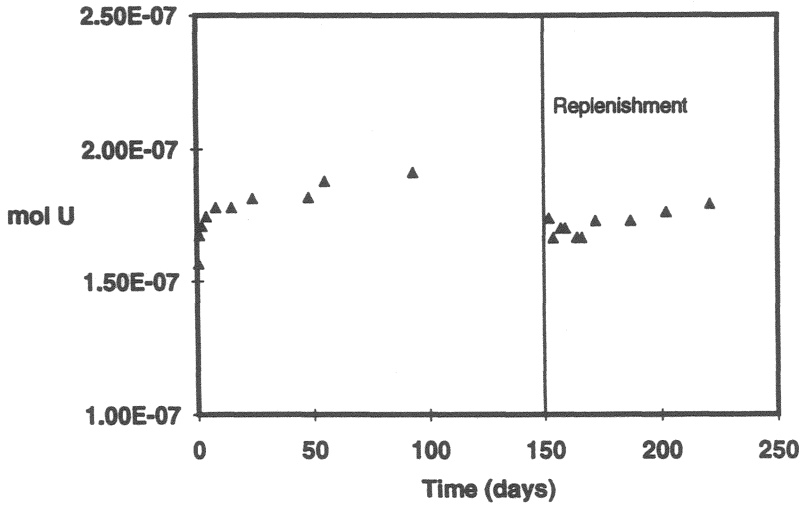

Fig. 2.2.2: Uranium concentration versus time in air (NaCl-brine).

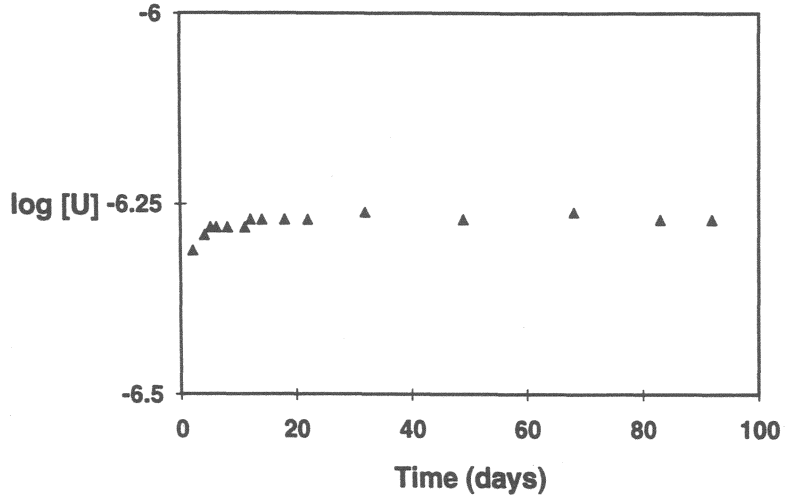

Fig. 2.2.3: Uranium concentration versus time in anoxic conditions (NaCl-brine in 100% nitrogen).

Under oxidizing conditions (fig 2.2.2), we have measured the dissolution rates before and after the replenishment. In this case, two different rates have been considered before the replenishment. The first one corresponds to the first four days of the experiment. The results are shown in the following table:

First dissolution rate	**73 10^{-8} mol/ d m^2**
Second dissolution rate	**3.2 10^{-8} mol/ d m^2**
Dissolution rate after replenishment	**2.6 10^{-8} mol/d m^2**

As it can be seen, the dissolution rate can be also attributed in this case to the dissolution of an oxidized layer. This oxidized layer would have a dissolution rate higher than the UO_2 under oxidizing conditions. It should be pointed out that we have obtained similar rates after the replenishment. This seems to indicate that the same surface is dissolving.

XPS surface analysis has been carried out with this solid to determine the final U(VI)/U(IV) ratio. In this case, we have obtained a surface of $UO_{2.4}$ which is close to the value obtained in diluted solution at the same pH. However, this value indicates that the final surface depends very much on pH because studies reported last years in Q-brine at pH=4 gave values near to $UO_{2.1}$. This result seems to point out that the dissolution mechanism in brines and in diluted solutions is similar.

Finally, in anoxic conditions (fig 2.2.3) a second dissolution rate lower than in oxidizing conditions can be calculated. This value is 6.2 10^{-9} mol/d m^2. In this case, the dissolution is very low and it is difficult at the present to distinguish it from a solubility value. More work is necessary to ascertain this difference.

2.2.3 REFERENCES

1.- Sunder S., Shoesmith D.W., Lemire R.J., Bailey M.G. and Wallace G.J., Corros. Sci., **32**, 373 (1991)
2.- Robbins J.C., Canad. Inst. Mineral. Mat. Bull., **5-61**, 2 (1978)
3.-Allen G.C., Tucker P.M. and Tyler J.W., J. Phys. Chem. **86**, 224 (1982)
4.-Casas I., Giménez J.,Martí V., Torrero M.E., and de Pablo J., Mat. Res. Soc. Symp. Proc. **294**, 61 (1993)
5.- Forsyth R.S. and Werme L.O., J. Nucl. Mater., **190**, 3 (1992)
6.- Ollila, K., "Results from Long-Term Dissolution Studies of Unirradiated UO_2 in Powered and Pellet form" presented at Spent Nuclear Fuel Workshop'93, Santa Fe, NM, September 1993.
7.- Johnson L.H., Shoesmith D.W., Lunansky G.E., Bailey M.G. and Tremaine P.R., Nuclear Technology, **56**, 238 (1982)
8.- Bruno J., Casas I. and Puigdomènech I., Geochim. Cosmochim. Acta, **55**, 647 (1991)
9.- Grambow B. and Müller, R., Mat. Res. Soc. Symp. Proc. **176**, 229 (1990)
10.- de Pablo J., Duro L., Giménez J., Havel J., Torrero M.E., Casas I., Anal. Chim. Acta, **264**, 115 (1992)